AGU PUBLICATIONS

JGR

Journal of Geophysical Research: Oceans

RESEARCH ARTICLE

10.1002/2015JC011156

Special Section:
Forum for Arctic Modeling and Observational Synthesis (FAMOS): Results and Synthesis of Coordinated Experiments

# Consequences of future increased Arctic runoff on Arctic Ocean stratification, circulation, and sea ice cover

**Aleksi Nummelin[1,2], Mehmet Ilicak[2,3], Camille Li[1,2], and Lars H. Smedsrud[1,2,4]**

[1]Geophysical Institute, University of Bergen, Bergen, Norway, [2]Bjerknes Centre for Climate Research, Bergen, Norway, [3]Uni Research Climate, Bergen, Norway, [4]Department of Arctic Geophysics, University Centre in Svalbard (UNIS), Longearbyen, Norway

**Key Points:**
- Larger river runoff leads to stronger Arctic Ocean stratification and warmer subsurface
- Arctic Atlantic Water circulation strengthens while net exchange with surrounding oceans decreases
- Volume outflow and ice export through the Fram Strait increase with the runoff

**Supporting Information:**
- Supporting Information S1
- Figure S1
- Figure S2
- Figure S3
- Table S1

**Correspondence to:**
A. Nummelin,
aleksi.nummelin@uib.no

**Citation:**
Nummelin, A., M. Ilicak, C. Li, and L. H. Smedsrud (2016), Consequences of future increased Arctic runoff on Arctic Ocean stratification, circulation, and sea ice cover, *J. Geophys. Res. Oceans*, *121*, 617–637, doi:10.1002/2015JC011156.

Received 30 JUL 2015
Accepted 15 DEC 2015
Accepted article online 18 DEC 2015
Published online 21 JAN 2016



**Abstract** The Arctic Ocean has important freshwater sources including river runoff, low evaporation, and exchange with the Pacific Ocean. In the future, we expect even larger freshwater input as the global hydrological cycle accelerates, increasing high-latitude precipitation, and river runoff. Previous modeling studies show some robust responses to high-latitude freshwater perturbations, including a strengthening of Arctic stratification and a weakening of the large-scale ocean circulation; some idealized modeling studies also document a stronger cyclonic circulation within the Arctic Ocean itself. With the broad range of scales and processes involved, the overall effect of increasing runoff requires an understanding of both the local processes and the broader linkages between the Arctic and surrounding oceans. Here we adopt a more comprehensive modeling approach by increasing river runoff to the Arctic Ocean in a coupled ice-ocean general circulation model, and show contrasting responses in the polar and subpolar regions. Within the Arctic, the stratification strengthens, the halocline and Atlantic Water layer warm, and the cyclonic circulation spins up, in agreement with previous work. In the subpolar North Atlantic, the model simulates a colder and fresher water column with weaker barotropic circulation. In contrast to the estuarine circulation theory, the volume exchange between the Arctic Ocean and the surrounding oceans does not increase with increasing runoff. While these results are robust in our model, we require experiments with other model systems and more complete observational syntheses to better constrain the sensitivity of the climate system to high-latitude freshwater perturbations.

## 1. Introduction

As the hydrological cycle accelerates in a warming climate, we expect increasing precipitation at high latitudes and increasing runoff to the Arctic Ocean. Observations show a 7% increase in Eurasian runoff from 1936 to 1999 [*Peterson et al*., 2002] that may well already have influenced Arctic Ocean circulation and stratification, and therefore also the sea ice cover. By the end of the century, climate model projections show a 30% increase in Arctic runoff (Figure 1) with an indication of an increase in both the freshwater storage in the Arctic Ocean and freshwater export to the North Atlantic [*Lehner et al*., 2012].

The Arctic Ocean (Figure 2) is strongly stratified, largely ice covered, and receives anomalously large freshwater input per unit area compared to the other world oceans [*Rudels*, 2015; *Rawlins et al*., 2010]. The Arctic Ocean stratification is characterized by a cold and fresh surface, a relatively warm and salty Atlantic Water layer at depth, and an intermediate layer of cold but gradually saltier water often termed the cold halocline [*Rudels et al*., 1996; *Steele and Boyd*, 1998; *Rudels et al*., 2004]. The fresh surface waters are derived from river runoff, positive net precipitation, relatively fresh Pacific inflow, and seasonal ice melt. The surface circulation is dominated by the transpolar drift crossing the Arctic Basin from the East Siberian and Laptev Seas to the Fram Strait, and the anticyclonic Beaufort Gyre in the Canada Basin. The cold halocline, derived from brine-enriched shelf waters and local winter convection, is most evident in the Canada Basin and largely absent in the Nansen Basin [*Rudels et al*., 1996; *Rudels*, 2015]. The warm Pacific inflow enters the upper halocline through Bering Strait, affecting the stratification mainly in the Canada Basin. Atlantic Water (AW) enters the Arctic Ocean in two branches, one through the Fram Strait and the other through the Barents Sea. The AW advects cyclonically around the basin creating an AW layer at depth through most of the Arctic Ocean [*Rudels*, 2015; *Jones*, 2001].

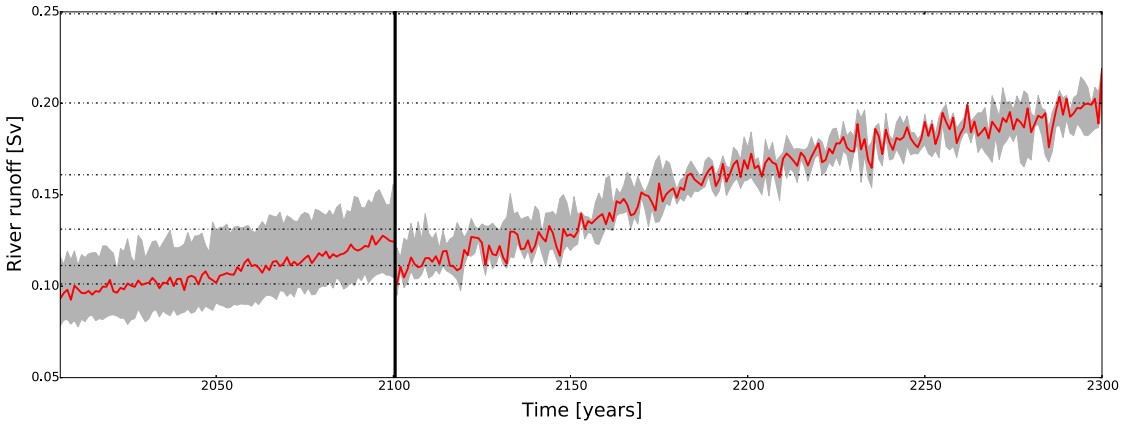


**Figure 1.** Expected annual mean runoff to the Arctic Ocean based on CMIP5 models using Representative Concentration Pathway (RCP) 8.5 (see supporting information Table S1 for models included in the ensemble). The red line shows the ensemble median, and the gray shading shows the interquartile range. The black dotted lines show the runoff values used in the idealized perturbation experiments (see Figure 3). The vertical line at year 2100 separates the period 2005–2100 with a large multimodel ensemble (19 models and total of 49 members) from the period 2100–2300 with a small ensemble (4 models and total of 6 members).

The variability in the pathways of Eurasian river runoff is largely governed by the Arctic Oscillation (AO), the leading mode of the atmospheric variability in the extratropical Northern Hemisphere. The AO influences the transpolar drift and the intensity of Ekman convergence to the Beaufort Gyre [*Morison et al*., 2012], both of which affect where freshwater tends to accumulate in the Arctic Basin. The bulk of the river runoff enters the vast Eurasian shelves and is transported mainly into the Canada Basin for a high AO index, but toward Fram Strait by the transpolar drift for a low AO index [*Morison et al*., 2012; *Alkire et al*., 2015]. Observations also suggest a linkage between the AO and the North American (mainly Mackenzie River) runoff pathways [*Yamamoto-Kawai et al*., 2009; *Fichot et al*., 2013]: there has been a shift from a rather direct outflow via the CAA in early 2000s to a northward pathway into the Beaufort Gyre around 2006 coinciding with a change to a strongly positive AO.

On the large scale, models respond to high-latitude freshwater perturbations with a slowdown of the oceanic circulation. In numerous hosing experiments, large amounts of freshwater are released over a 50°N–70°N latitude band in the subpolar North Atlantic Ocean. Such a freshwater perturbation reduces convection in the North Atlantic, slows down the surface circulation and Atlantic Meridional Overturning Circulation (AMOC), and reduces the northward ocean heat transport [*Manabe and Stouffer*, 1995; *Stouffer et al*., 2006; *Stocker et al*., 2007], as well as leading to a subsurface warming in the North Atlantic and Arctic Oceans [*Mignot et al*., 2007]. Similar results are achieved using more realistic perturbations with both Greenland meltwater [*Gerdes et al*., 2006; *Swingedouw et al*., 2014] and Arctic river runoff [*Rennermalm et al*., 2006, 2007]. In fact the large-scale ocean and climate response is found to be similar to that described above whenever the freshwater forcing originates upstream of the North Atlantic convection sites [*Roche et al*., 2010] while a qualitatively different response is found if the forcing is applied downstream of the convection sites [*Mignot et al*., 2007].

The local effects of Arctic river runoff have been studied in more detail using both observations and a variety of models. Idealized regional modeling work links surface freshening to stronger currents inside the Arctic Ocean [*Spall*, 2013], and high-resolution modeling work finds that increasing runoff induces stronger currents close to river mouths [*Whitefield et al*., 2015]. Runoff also affects the sea ice cover and dense water production in the shelf seas as well as the large-scale hydrography inside the Arctic Basin. More river runoff has been linked to more summer melt, but also to earlier freezing in both observations [*Bauch et al*., 2013; *Nghiem et al*., 2014] and modeling studies [*Whitefield et al*., 2015]. Observations also indicate that less river water on the shelf can increase local bottom water production [*Dmitrenko et al*., 2010]. Finally, *Nummelin et al*. [2015] showed that the density and temperature stratification of the Arctic Ocean are tightly linked: under stronger freshwater forcing, the large-scale hydrography approaches a steady state with a warmer subsurface, but stronger density stratification that together balance the vertical heat flux.

The overall effect of increasing runoff on the climate system requires a combined understanding of the local Arctic processes and those linking the Arctic to the surrounding oceans. While the large-scale response of the climate system to high-latitude freshwater perturbation in the Atlantic is rather well documented, the

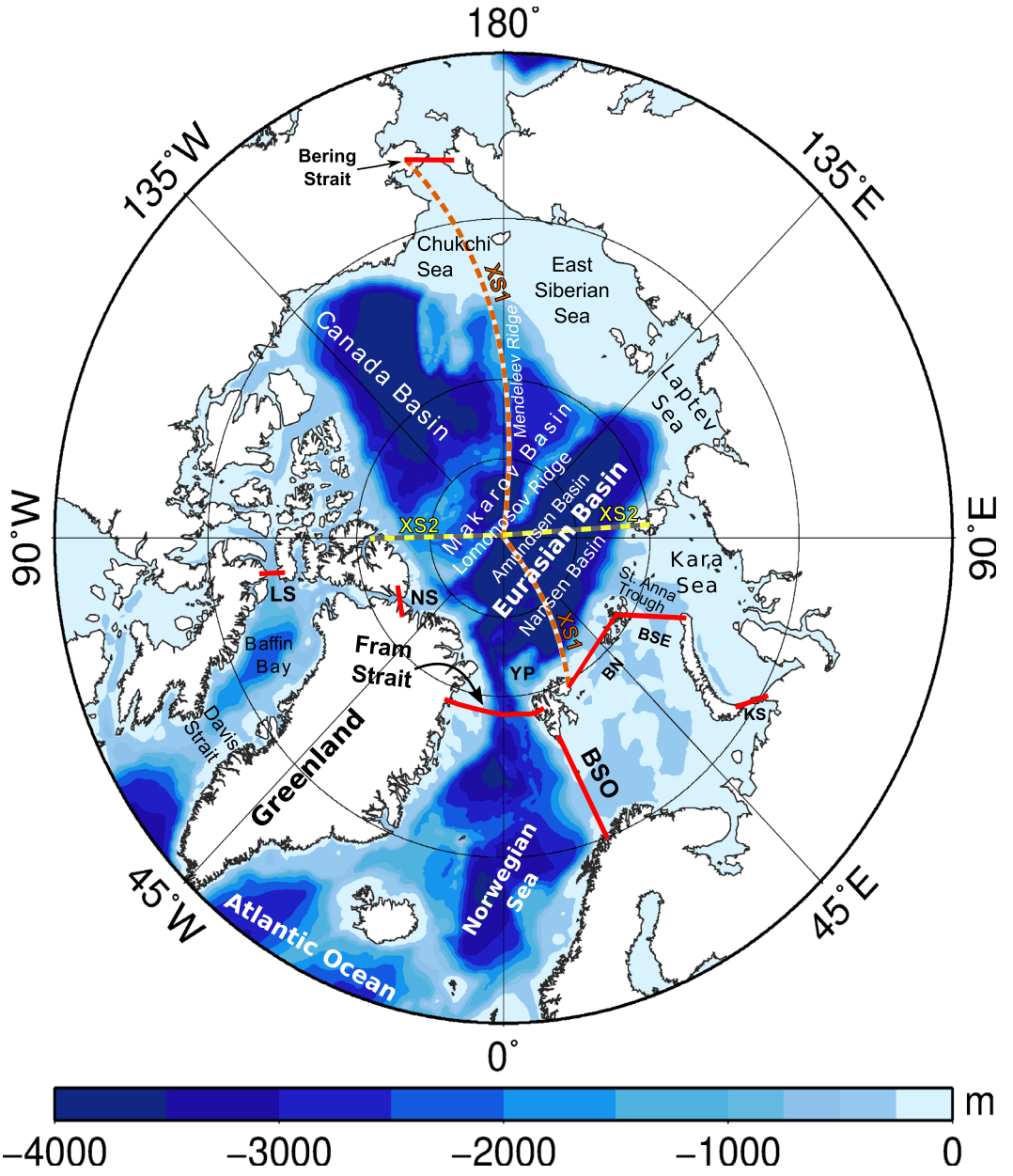


**Figure 2.** Arctic Ocean bathymetry. Main basins and connecting gateways are labeled. Abbreviations are: BSO, Barents Sea Opening; BN, Barents North; BSE, Barents Sea Exit; KS, Kara Strait; LS, Lancaster Sound; NS, Nares Strait. Labels XS1 and XS2 correspond to the cross sections shown in Figures 8 and 9.

regional response of circulation and hydrography in the Arctic Ocean has not been previously studied outside idealized settings. The conditions in the Arctic are strongly influenced by lower latitudes and vice versa, creating important oceanic connections that are as yet unexplored.

In this study, we use a coupled ocean-sea ice general circulation model to show two distinct responses to increasing Arctic runoff: (a) a spin-up of the circulation and warming in the Arctic Mediterranean, and (b) a slowdown and cooling south of the Greenland-Scotland ridge in the North Atlantic. Inside the Arctic Ocean, neither the dynamic nor thermodynamic response can be understood simply by a reduction in AMOC. For the North Atlantic, our results are largely consistent with previous freshwater hosing studies [*Stouffer et al.*, 2006; *Stocker et al.*, 2007; *Mignot et al.*, 2007; *Roche et al.*, 2010].

The paper is structured as follows: we describe the modeling strategy along with the control simulation in section 2; analyze the Arctic and large-scale oceanic responses to increasing runoff in section 3;

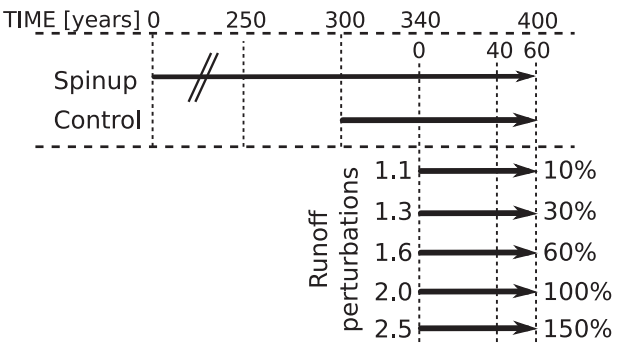


**Figure 3.** Design of spin-up and perturbation experiments. The labels 1.1–2.5 (10%–150%) indicate the factor (percentage) of runoff increase relative to the control run.

discuss our results in the context of earlier work in section 4; and present concluding remarks in section 5.

## 2. Model and Methods

### 2.1. Experimental Setup

In this study, we use the coupled ocean-sea ice component of the Norwegian Earth System Model (NorESM) [*Bentsen et al.*, 2013]. We use the bipolar grid with 1° nominal resolution previously used in the Coupled Model Intercomparison Project Phase 5 (CMIP5) for both ocean and sea ice components. The ocean component is based on Miami Isopycnic Coordinate Ocean Model (MICOM) [*Bleck and Smith*, 1990; *Bleck et al.*, 1992] with 51 isopycnic vertical levels and 2 levels with freely evolving density at the surface mixed layer. The ocean model has an Arakawa C discretization in the horizontal and uses leapfrog time stepping. The ocean model formulation is mass conserving (non-Boussinesq), but for simplicity, the transports are shown in units of volume transport (1 Sv = 1E6 $m^3$ $s^{-1}$) and the conversion is done simply by dividing the mass transport by a factor of 1E9 kg $m^3$ $s^{-1}$/Sv. The sea ice model is the version of the Los Alamos sea ice model (CICE4) [*Gent et al.*, 2011; *Holland et al.*, 2012] used in NorESM and the Community Climate System Model version 4 (CCSM4). The model is forced with the Coordinated Ocean-ice Reference Experiments (CORE) Normal Year Forcing (NYF), which is based on the 1958–2000 period [*Large and Yeager*, 2004], i.e., the atmospheric forcing is a repeating climatological year. Outgoing surface fluxes are calculated with bulk formulas, and incoming radiation is affected by changes in surface albedo (sea ice cover). River runoff is treated as a virtual salinity flux. A more detailed model description can be found in sections 2.3 and 2.4 of *Bentsen et al.* [2013].

The model is spun-up for 340 years in a two-stage process (Figure 3). The model starts from rest and is run first for 300 years with sea surface salinity (SSS) restored toward CORE climatological SSS. Due to lack of atmospheric feedbacks, the restoring term is necessary to keep model salinities from drifting too far from observations. The variable restoring term is forced to stay below $\pm$3.52E-3 m $s^{-1}$ and for this first period, the restoring time scale is 6 days. To avoid generating large variability via the SSS restoring, we calculate a restoring climatology from years 250 to 300 and apply the climatological restoring together with a greatly reduced variable restoring (restoring time scale of 60 days, 10% of the variable restoring used for spin-up). This makes for a close to constant SSS restoring term so that the differences between the runs are not primarily due to the SSS restoring. Using the new SSS restoring, we run the model for another 40 years (until 340 years). We scale the magnitude of the restoring term down to zero at the river mouths by multiplying it with a mask (Figure 4a) that leaves the Arctic SSS largely free to evolve as we change the runoff.

At 340 years, we start the runoff experiments. We increase the runoff in the Arctic while using control runoff values elsewhere (Figure 4b). We ran five different perturbation experiments (Figure 3) with runoff increases of 10%, 30%, 60%, 100%, and 150% compared to the control simulation, which has close to 0.1 Sv freshwater runoff entering the Arctic Ocean via rivers. Note that we do not increase melting from Greenland. The runoff perturbations are applied for 60 years (from year 340 to 400) and unless otherwise specified results are shown for the last 20 years of the simulation (Figure 3). Significance is also calculated over the last 20 years using a Welch test. The freshwater content is calculated relative to a reference salinity of 34.8. During the 20 year analysis period, the Arctic Ocean hydrography and circulation have largely equilibrated, but the deep ocean is still adjusting. For example, the maximum AMOC in most of the perturbation experiments shows a downward trend (approximately 1.5 Sv/decade for the 2.0 experiment).

Runoff seasonality is of minor importance for the time and spatial scales in this study and is not taken into account. River water resides on the shelves for several years [*Schlosser et al.*, 1994; *Bauch et al.*, 2013]. The runoff-induced annual cycle in salinity is very small away from river mouths and is therefore not of first-order importance for the large-scale ocean response. Furthermore, in the future, the runoff is expected to be more equally distributed throughout the year. In a warmer climate, reduced snow cover leads to reduced

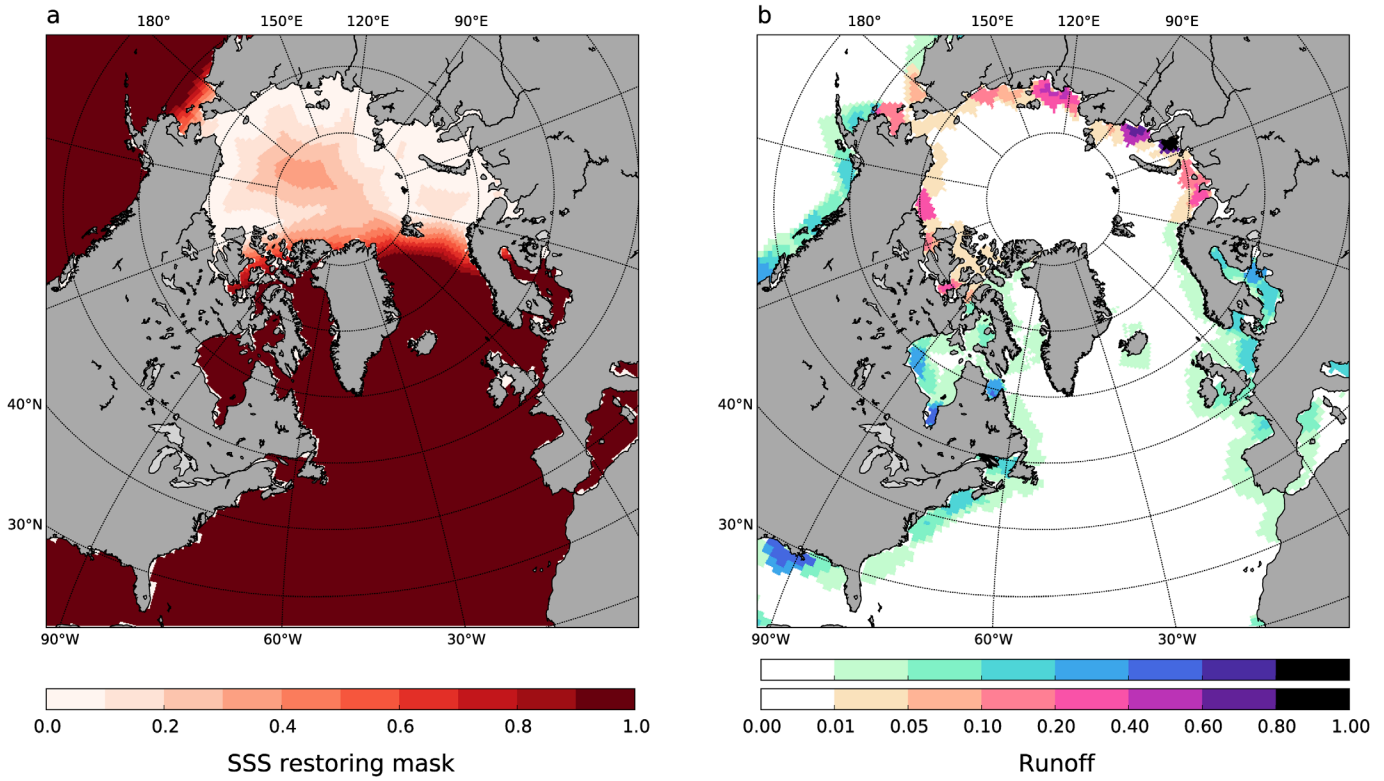


**Figure 4.** (a) Sea surface salinity restoring mask and (b) runoff forcing field. In Figure 4b, warm colors denote areas where the runoff increase is applied, and cool colors denote areas where runoff is kept at control levels. The intensity of the color denotes the strength of the runoff in both cases. Runoff values are normalized by the maximum value inside the Arctic Basin.

spring peak discharge while increases in winter (liquid) precipitation and snow melt lead to more winter runoff [*Rennermalm et al.*, 2010; *Overeem and Syvitski*, 2010]. We note that for shelf processes near the river mouths, the changing seasonality might bear some importance [*Bauch et al.*, 2013; *Whitefield et al.*, 2015], but these processes cannot be captured accurately in ocean models with 1° horizontal resolution and are thus beyond the scope of this work.

The main atmospheric feature of potential importance for the Arctic runoff distribution is the AO. The AO is a pattern of atmospheric variability commonly defined as the first Empirical Orthogonal Function (EOF) of monthly sea level pressure anomalies north of 20°N. *Morison et al.* [2012] argued that a positive AO pattern can lead to accumulation of Eurasian runoff in the Beaufort Gyre while a negative AO pattern drives the Eurasian runoff directly toward Fram Strait. We apply CORE NYF atmospheric forcing based on the 1958–2000 climatology, a period during which the mean AO was close to neutral (−0.12 using monthly data from http://www.cpc.ncep.noaa.gov/products/precip/CWlink/daily_ao_index/monthly.ao.index.b50.current.ascii). The implications of this are discussed in section 4.3.

For most of the analysis and graphics, we use the software packages matplotlib [*Droettboom et al.*, 2015; *Hunter*, 2007] and Physical Analysis of Gridded Ocean data (PAGO; available at http://www.whoi.edu/science/PO/pago/index.html [*Deshayes et al.*, 2014]).

### 2.2. Control Simulation

The simulated sea surface temperature (SST) and sea surface salinity (SSS) are in qualitative agreement with observations at large scales. Figure 5 shows simulated annual mean patterns compared to the World Ocean Atlas (WOA) 2013 [*Locarnini et al.*, 2013; *Zweng et al.*, 2013] in the Atlantic-Arctic sector. The main discrepancies relevant for this study are found in the Gulf Stream region and in the Arctic Ocean. The Arctic shelf regions are generally too cold and saline when compared to the observations (Figure 5b). This could be because the model mixed layer parameterization produces an overly cold, deep, and consequently saline mixed layer. In addition, sparse, summer-biased observations and large interannual variability in these

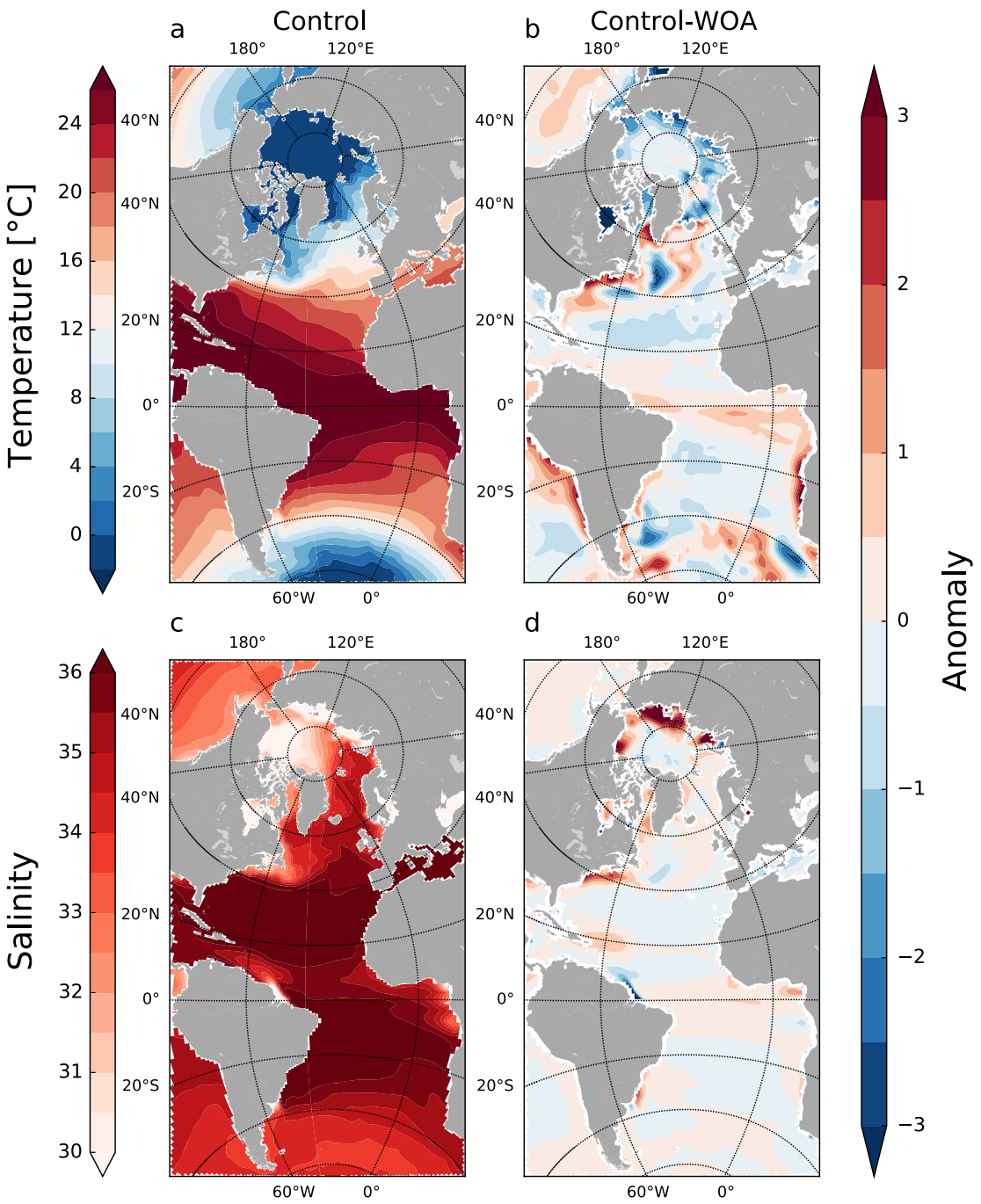


**Figure 5.** (a, c) Annual mean surface temperature and salinity in the control simulation, and (b, d) the anomalies between the control simulation and WOA13 climatology [*Locarnini et al.*, 2013; *Zweng et al.*, 2013]. The largest temperature and salinity biases in the Arctic shelf regions are −4.4°C and 7.9 psu, respectively.

regions make direct data-model comparison difficult. In fact, comparison with other observational data sets (MIMOC [*Schmidtko et al.*, 2013] and PHC3.0 updated from *Steele et al.* [2001]) shows discrepancies of opposite sign in some shelf regions (supporting information Figures S1 and S2). The Gulf Stream is too far south, resulting in substantial SST differences compared with the WOA in the North Atlantic. The east coast of North America is too warm, likely because the horizontal resolution there is too low to correctly resolve the spreading of cold waters from the north along the coast with the Nova Scotia Current, and because the lateral mixing with the warm offshore waters might be overly large in the model.

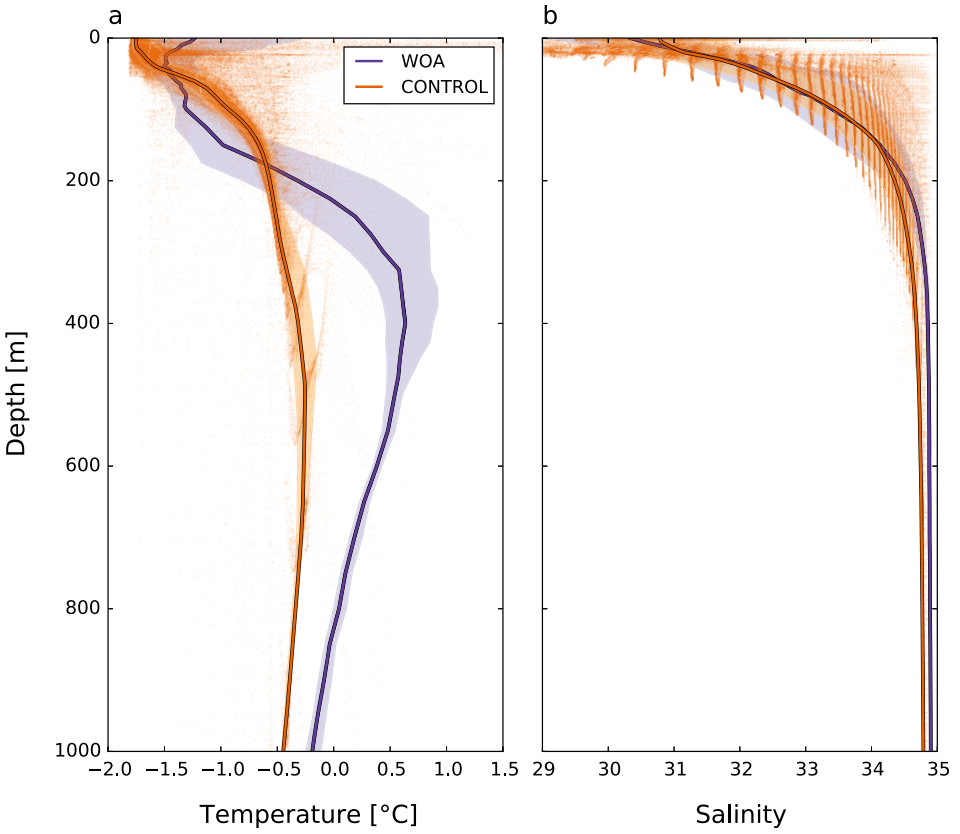


**Figure 6.** Vertical profiles of annual median (a) temperature and (b) salinity averaged over the Arctic Ocean (excluding the Barents Sea) for the control simulation and the WOA13 climatology [*Locarnini et al*., 2013; *Zweng et al*., 2013]. Shading shows the interquartile range while the dots show the individual grid cell values.

The simulated vertical stratification in the Arctic suffers from issues that are well known among coarse resolution models. Figure 6 shows simulated and observed vertical mean profiles of temperature and salinity for the Arctic Basin. The main biases are an overly cold surface, an overly warm halocline (Upper Polar Deep Water) and an AW layer that is too cold and fresh. The deficiencies in the vertical structure are common to many models with similar resolution and they are linked to too much vertical mixing in the Arctic Ocean [*Komuro*, 2014; *Pemberton et al*., 2015] and poor treatment of the brine released from sea ice formation [*Nguyen et al*., 2009].

The net volume exchanges in the Arctic gateways are close to observations (Table 1). The simulated net transport to the Arctic Ocean through the Barents Sea Opening (BSO; 2.45 Sv) is similar to the observed estimate (2.3 Sv), while the net transport through Fram Strait (−1.39 Sv) is smaller than observations indicate (−2.0 Sv). Note that the slightly negative (out of the Arctic) net transport through Fram Strait is the sum of much larger inflow and outflow terms that are not as well simulated. The simulated AW inflow through the Fram Strait and BSO combined is only $7.8 \pm 0.1$ Sv, of which the Fram Strait alone contributes $3.9 \pm 0.1$ Sv. The most recent observational estimate for the Fram Strait inflow is $6.6 \pm 0.4$ Sv [*Beszczynska-Möller et al*., 2012]. It is likely that the small Fram Strait inflow contributes to the discrepancies in the vertical profiles, especially the cold bias in the AW layer. The Bering Strait inflow (0.8 Sv) and CAA outflow (2.0 Sv) compare well with observations. However, the two main CAA gateways, Nares Strait and Lancaster Sound, have close to equal contributions to the outflow from observations [*Melling et al*., 2008], while the simulated Nares Strait contribution is 3 times larger than that of Lancaster Sound. The surface circulation and AW circulation in the Eurasian Basin (supporting information Figure S3b) in the control simulation are in qualitative agreement with observations, but the weak anticyclonic AW layer circulation in the Canada Basin (supporting information Figure S3) is likely a result of a long-term adjustment to relatively strong Beaufort Gyre (similar to response to strong Beaufort Gyre in *Karcher et al*. [2007]).

**Table 1.** Net Volume and Heat Transports in Arctic Gateways[a]

| Source | Fram Strait | BSO | Bering Strait | CAA | Davis Strait |
|---|---|---|---|---|---|
| | | *Volume Transport (Sv)* | | | |
| NorESM | −1.39±0.04 | 2.45 ± 0.02 | 0.94 ± 0.00 | −2.0±0.02 | −2.0±0.02 |
| *Woodgate et al.* [2005] | | | 0.8 | | |
| *Melling et al.* [2008] | −2.0 | 1.8 | 0.8 | 1–2 | 3 |
| *Smedsrud et al.* [2013] | | 2.3 | | | |
| *Schauer et al.* [2008] | −2.0 | | | | |
| | | *Heat Transport (TW)* | | | |
| NorESM | 26.49 ± 0.75 | 57.32 ± 0.43 | 5.15 ± 0.06 | 7.75 ± 0.07 | |
| *Schauer et al.* [2008] | 26−50 | | | | |

[a]NorESM values are mean transports over the last 20 years of the control simulation ± standard deviation. All other values are observational estimates.

## 3. Results

The main Arctic Ocean responses to increased runoff are a fresher surface, a warmer halocline, and a warmer AW layer. These responses are visible in Figure 7 showing the median temperature and salinity profiles over the deep Arctic Basin. The increased runoff leads to stronger stratification, which in turn sharpens the temperature gradient across the halocline. Deeper down, the AW layer becomes warmer and rises in the water column. These first-order results are consistent with previous idealized modeling efforts [*Nummelin et al.*, 2015; *Nilsson and Walin*, 2010].

In this section, we examine the response to increasing runoff in terms of the changes in the local stratification (section 3.1), the local circulation (section 3.2), the inflows and outflows to the Arctic Ocean (section 3.3), and the large-scale ocean circulation (section 3.4). We focus on the 2.0 runoff experiment, i.e., a doubling of present-day runoff that is projected to occur by the end of the 23rd century (Figure 1), because the responses shown are largely linear to runoff amount.

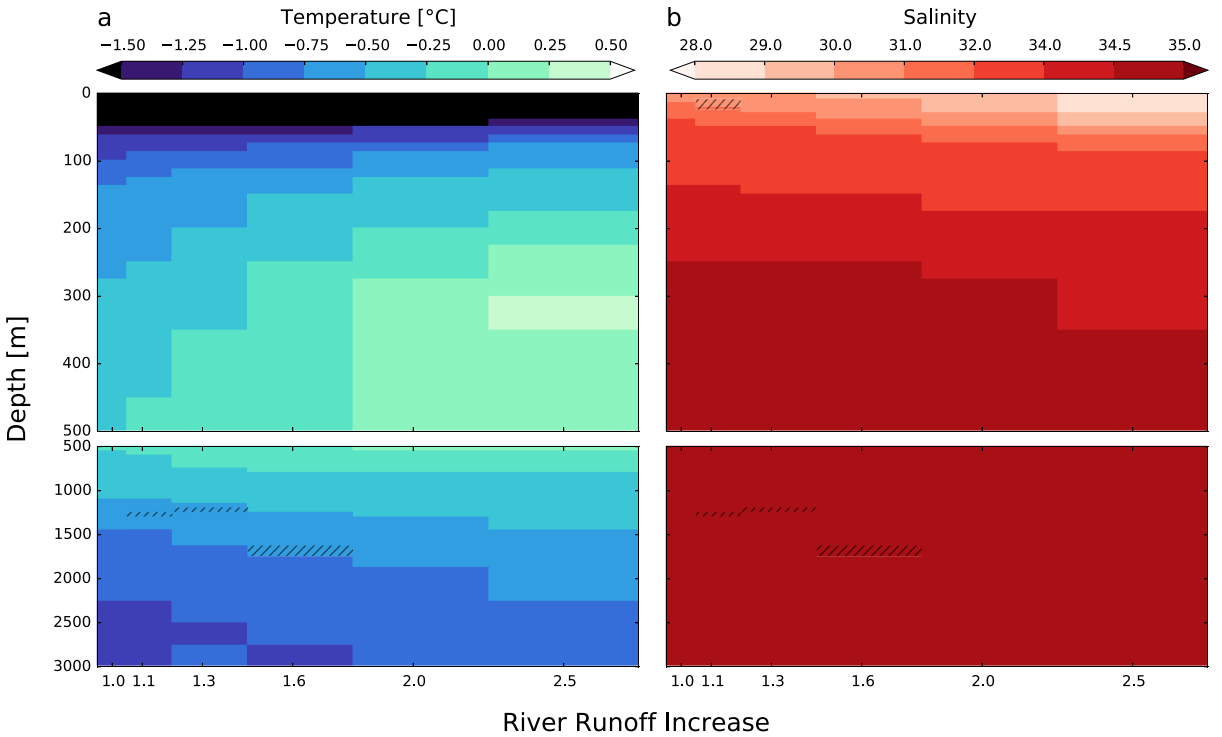


**Figure 7.** Vertical profiles of annual median (a) temperature and (b) salinity as a function of runoff averaged over the Arctic Ocean (excluding the Barents Sea). Hatching indicates values that are not significantly different from the control simulation at the 95% confidence level.

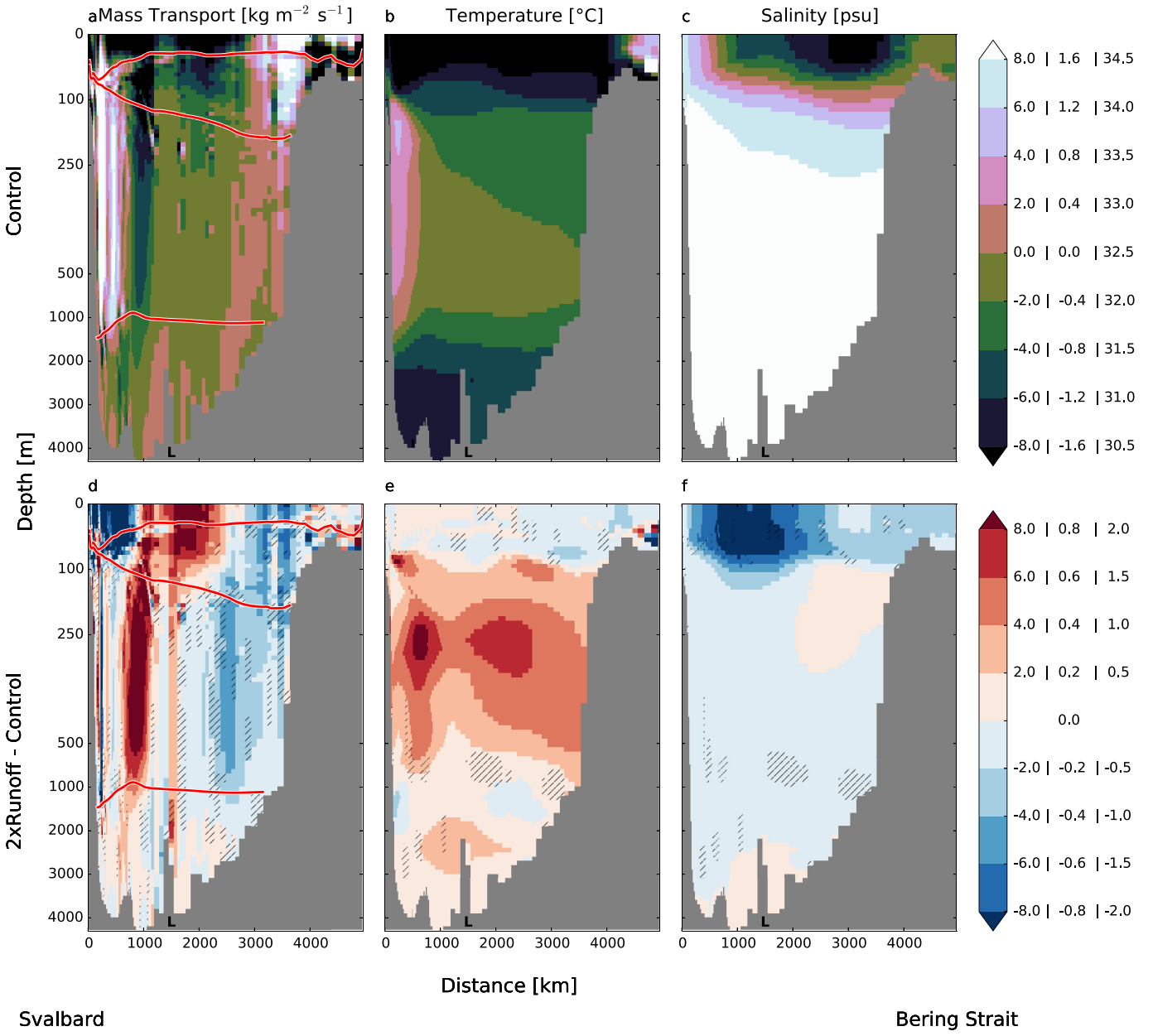


**Figure 8.** Cross-section XS1 through the Arctic from (left) Svalbard toward (right) Bering Strait showing (left) transport (positive values indicate flow toward Eurasia, and negative values indicate flow toward North America), (middle) temperature, and (right) salinity. The L in each plot indicates the location of the Lomonosov ridge. Figures 8a–8c show vertical profiles from the control simulation, and Figures 8d–8f show anomalies in the 2.0 runoff experiment (2.0 × runoff – control). Note that the transport anomalies are not absolute so a negative anomaly can indicate either stronger flow toward Eurasia or weaker flow toward North America. The color bar labels apply to the plot in the respective column (i.e., the left set of labels are for the mass transport, etc.). Hatching indicates values that are not significantly different from the control simulation at the 95% confidence level. The red lines in Figures 8a and 8d show boundaries of the surface mixed layer (model layers 1–2, approximately 0–50 m) and AW layer (model layers 33–45, approximately 100–1000 m) used in Figure 12. The cross-section XS1 is indicated on the map in Figure 2.

### 3.1. Changes in Arctic Hydrography

The hydrographic response to increased river runoff is a surface freshening and subsurface warming through the entire Arctic Ocean. In the Eurasian Basin north of Svalbard (Figures 8b and 8e), the warm anomaly is evident throughout the AW layer and peaks at around 1°C. In the Canada Basin, the anomaly continues to extend from Siberia to the CAA along the cyclonic flow path (Figures 8b, 8e, 9b, and 9e).

There is another, shallower warm core in the halocline (at about 100 m depth) throughout most of the Arctic Ocean (Figures 8–10c, and 10d). The warmer halocline is a result of changes on the shelves. In the control

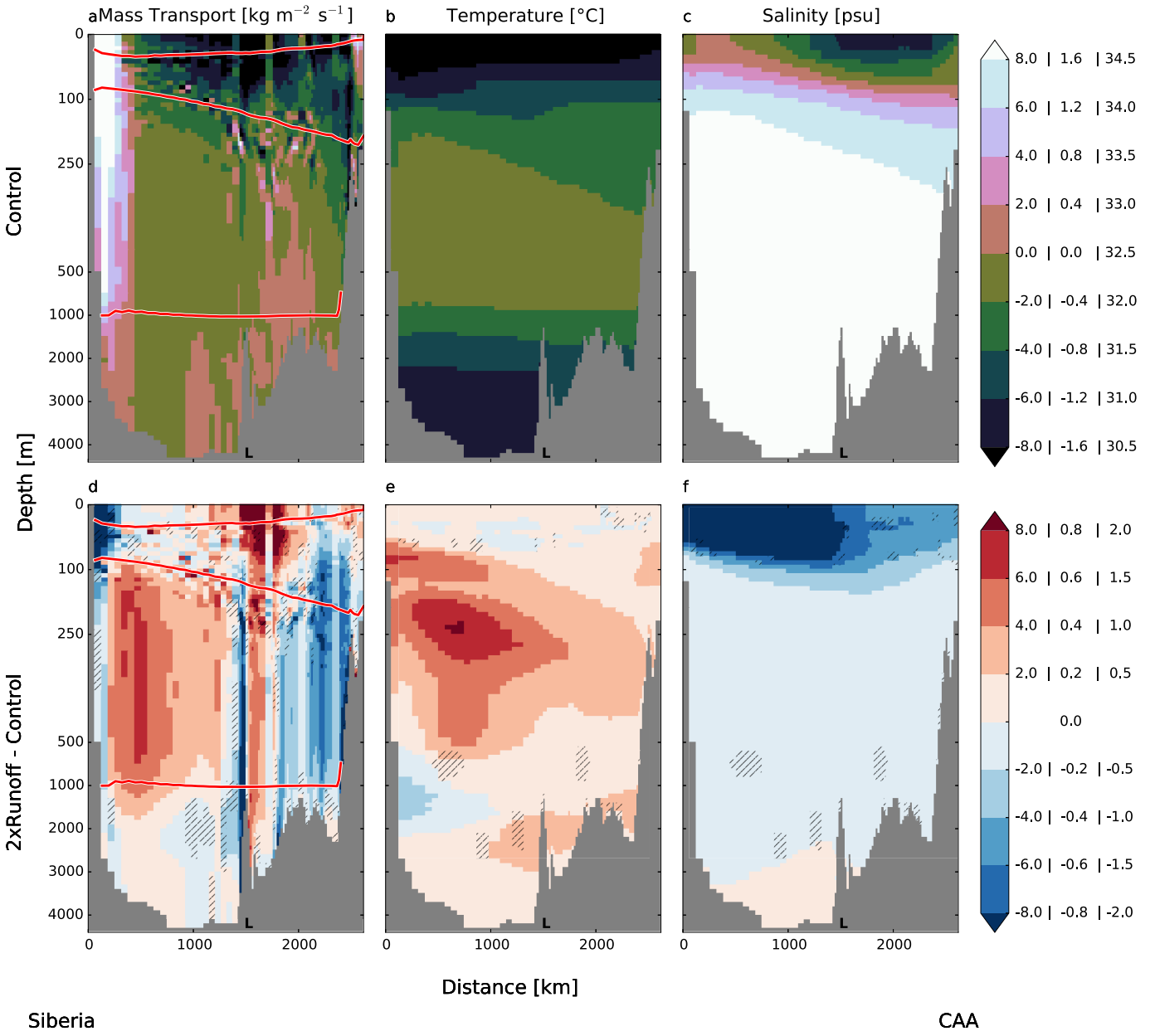


**Figure 9.** Same as Figure 8 but for cross-section XS2 through the Arctic from (left) Siberia to (right) the CAA.

simulation, the lowest temperatures in the central Arctic halocline are found off the Barents Sea and the Siberian shelves, indicating a flow of cold dense waters from the shelves toward the interior Arctic Ocean (Figure 10c). When the runoff is doubled, the coldest regions off and on the shelves become warmer (Figure 10d), indicating reduced cooling over the shelf regions due to stronger stratification. The cold anomaly off the Chukchi Shelf is related to reduced heat transport through Bering Strait and redistribution of fresher (and lighter), but still cold, shelf waters higher in the water column (see also the temperature and salinity signals in Figure 8).

Like the warmer halocline, the warmer AW layer also arises from processes internal to the Arctic Ocean. In the control simulation, the AW layer flows through the Fram Strait as a relatively warm current, but cools quickly as it flows along the northern slope of the Barents Shelf (Figure 10e). The cooling is a direct consequence of mixing with cold shelf waters, and heat loss to ice melt and the atmosphere. In the 2.0 runoff experiment, the AW layer is generally colder as it enters the Arctic Ocean (through the eastern Nordic Seas), but it is not cooled

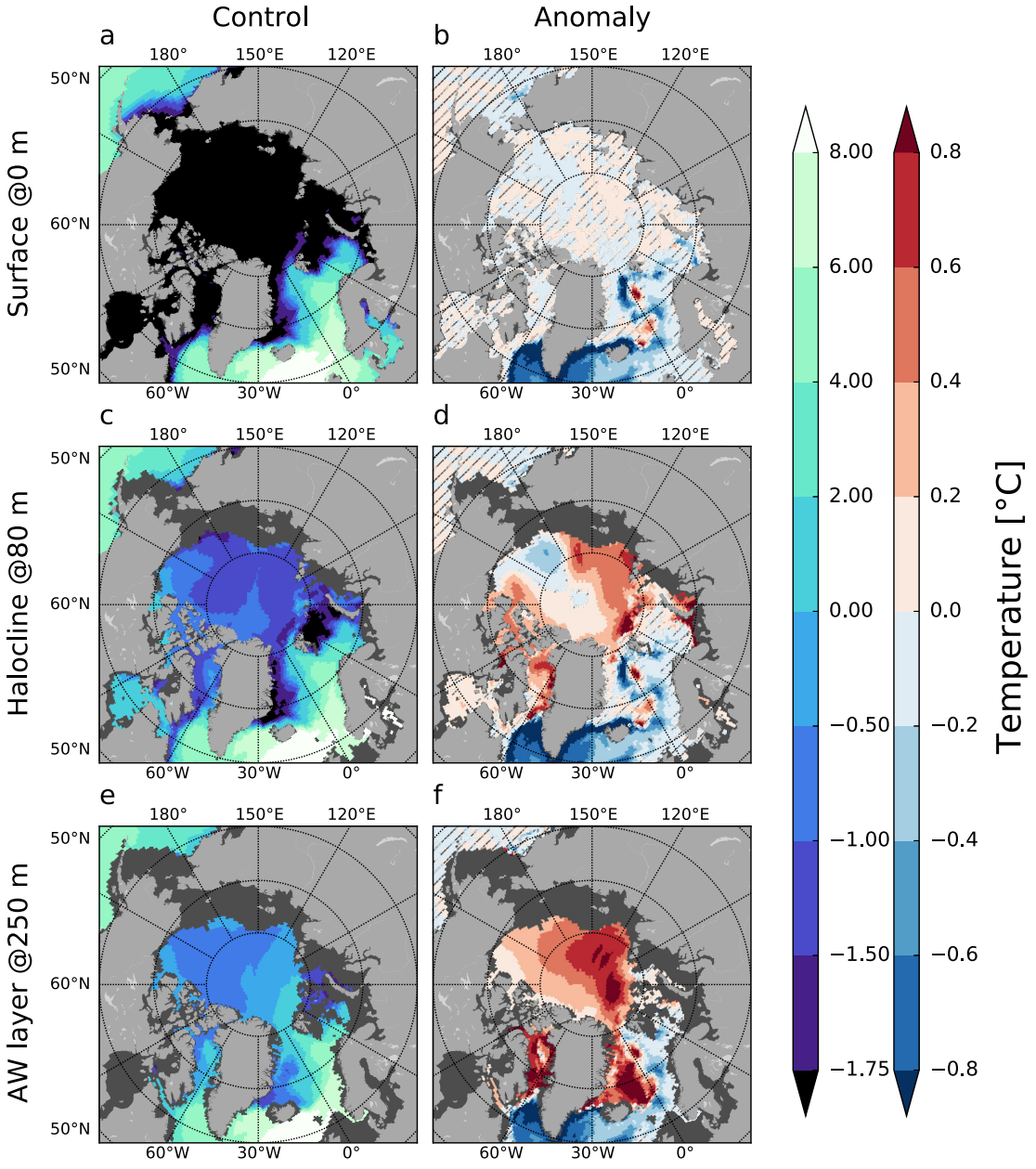


**Figure 10.** Winter (January to March) temperatures in the control simulation and anomalies in the 2.0 runoff experiment (2.0 runoff-control) at the (a, b) surface, (c, d) halocline (at 80 m depth), and (e, f) AW layer (at 250 m depth). Hatching indicates values that are not significantly different from the control simulation at the 95% confidence level. The left colorbar is for the control simulation and the right colorbar is for the anomalies.

as effectively as in the control simulation due to stronger stratification and warmer shelf waters (Figure 10f, see also section 3.4). Consequently, a warm anomaly develops further inside the Arctic Ocean.

Sea ice thickness changes are generally modest owing to competing effects in the perturbation experiments. The sea ice response is consistent throughout the year, and shows little seasonal difference within each region (Figure 11). There are thickness decreases in select places in the Eurasian Basin, and general increases in the Canada Basin, with the largest increases occurring close to the shelf break at Chukchi and East Siberian Seas, a region with a strong ice thickness gradient. For the Canada Basin, weaker Beaufort Gyre (see section 3.2) allows for a longer residence time of ice, increasing both the thickness and age of the ice in the Canada Basin, while for the Eurasian Basin, larger ice export through Fram Strait (approximately 9.5% or 5.5E3 $m^3$ $s^{-1}$ increase in the 2.0 perturbation experiment) tends to thin ice. The stronger

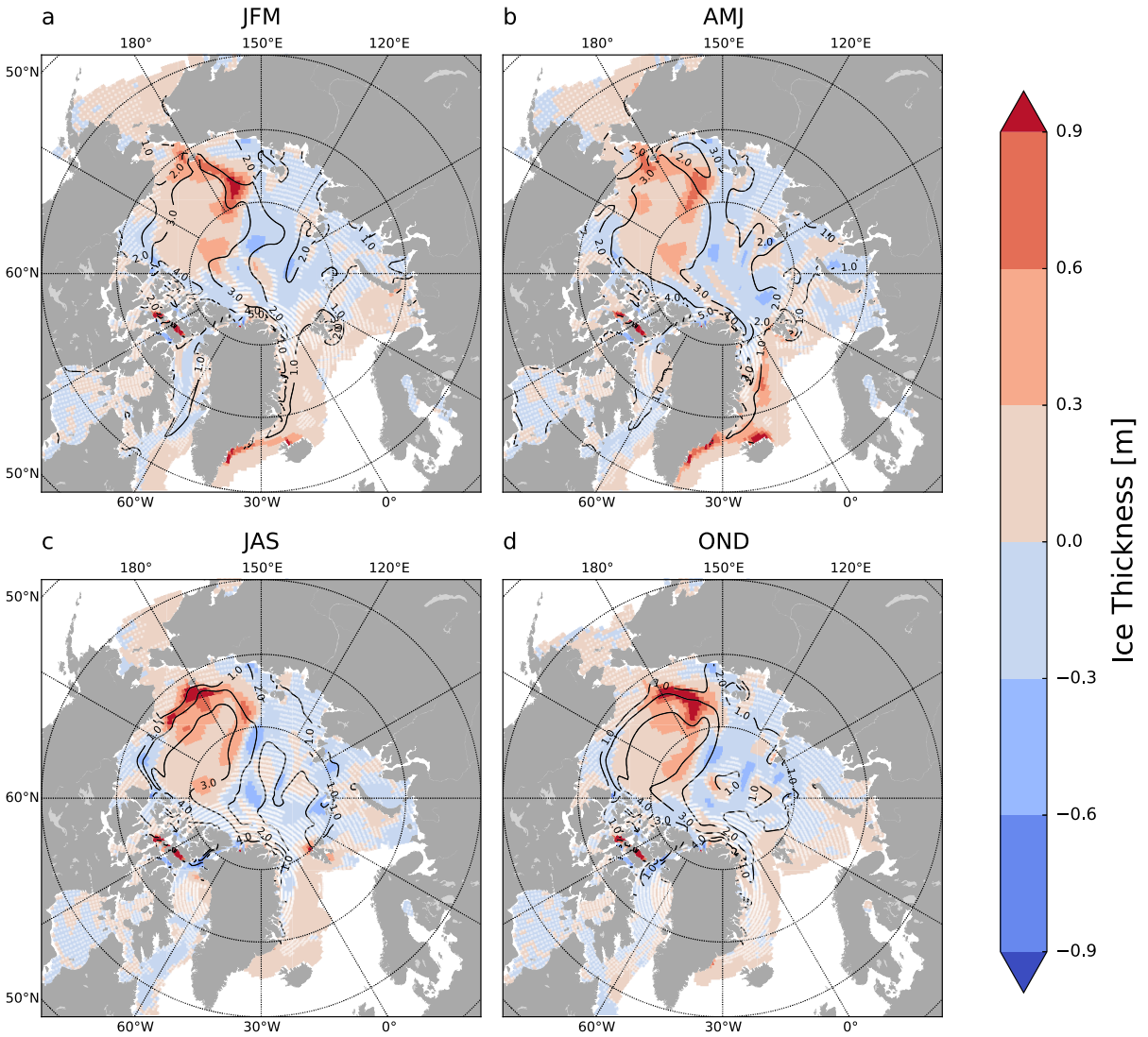


**Figure 11.** Seasonal mean sea ice thickness anomalies in the 2.0 runoff experiment compared to the control simulation. Ice thickness in the control simulation is shown in black contours (m). White stippling shows areas where the anomaly is not statistically significant at the 95% level. Seasons: JFM is January to March, AMJ is April to June, JAS is July to September, and OND is October to December.

stratification and reduced Bering Strait inflow favor thermodynamic growth, but actual changes in ocean to ice heat flux (not shown) are generally small. Because we used a standalone sea ice-ocean model, the ice area is to a large extent bound by the atmospheric forcing, which remains constant in our simulations. In a fully coupled simulation, atmospheric temperatures would respond to changing sea ice cover and reinforce the ice changes, for example, expanding ice would cool the atmosphere and reduced ice would warm the atmosphere. The large-scale atmospheric circulation would also be affected through thermodynamic coupling (higher pressure over cold ice-covered surface) and dynamic coupling (changing surface momentum exchange depending on the ice area and thickness). Finally, we do not account for sea ice decline due to increased greenhouse gas concentrations.

### 3.2. Changes in Circulation Within the Arctic Ocean

Under increased runoff, the barotropic flow intensifies in the Eurasian Basin and weakens in the Canada Basin, reflecting changes in the surface and deep circulation (Figure 12a). The stronger barotropic stream function in the Eurasian Basin results from the Arctic-wide strengthening of the cyclonic boundary current circulation in the AW layer (Figure 12c). The weaker barotropic circulation in the Canada Basin is the

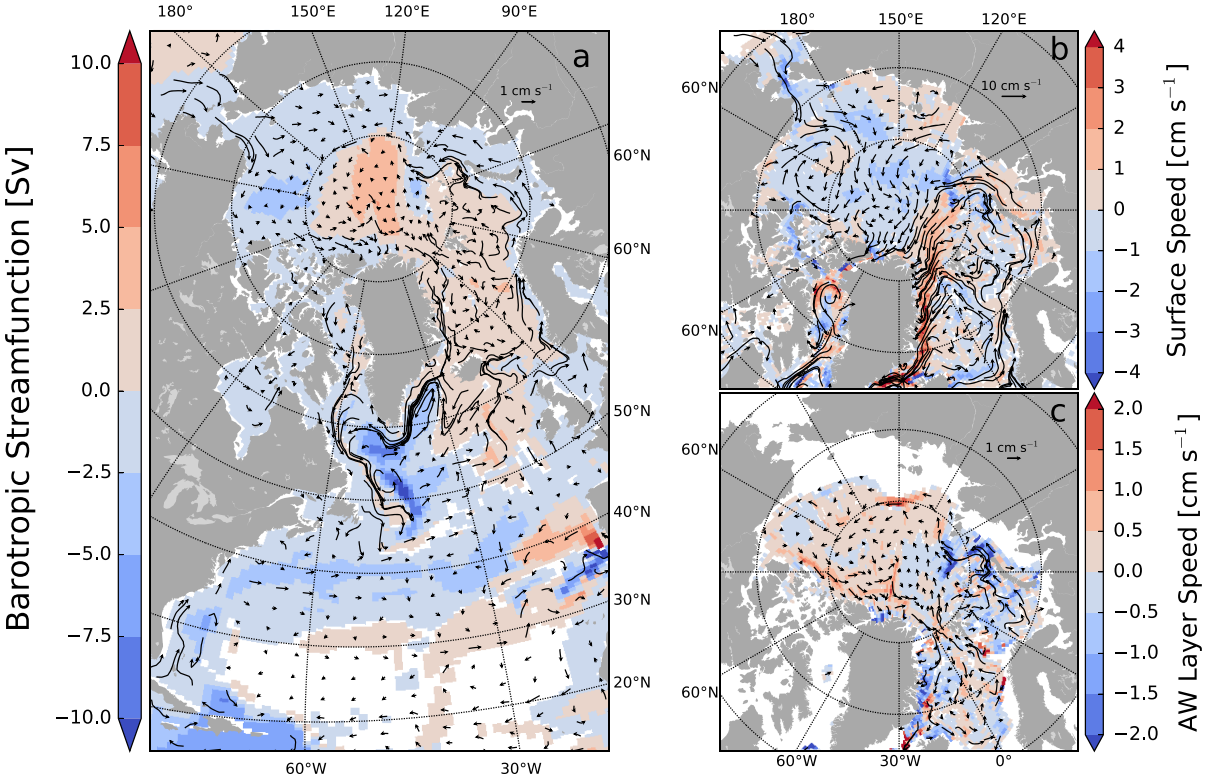


**Figure 12.** Ocean circulation in the 2.0 runoff experiment (vectors) and anomalies compared to the control simulation (shading): (a) barotropic stream function, (b) surface current speed in model layers 1–2 (approximately 0–50 m depth), and (c) AW layer current speed in model layers 33–45 (approximately 100–1000 m depth). Only anomalies that are significant at the 95% confidence level are plotted. Note that Figures 12b and 12c show the anomalies in current speed (absolute velocity) which is different from Figures 8 and 9 where we show anomalies in the mass transport.

combined result of the opposite responses in the surface (Figure 12b, weaker anticyclonic Beaufort Gyre) and AW layer (Figure 12c, stronger cyclonic) circulation. The weakening of the Beaufort Gyre (Figure 12b) and associated shift in the transpolar drift toward the Eurasian Basin (Figures 8 and 9) are due to a weakening of the sea surface height (SSH) gradient (Figures 14a and 14b) between the Canada Basin and Eurasian Basin.

The intensified flow in the AW layer (Figures 8 and 9, and 12c) is a result of the stronger stratification, which leads to sharper horizontal density gradients [*Spall*, 2013] and reduces the atmospheric (anticyclonic) momentum transfer to the ocean [*Lique et al*., 2015]. Lighter waters produced at the Barents Shelf weaken the gravity current entering St. Anna trough (Figure 12c). There is also a widening of the boundary current which could indicate stronger eddy momentum transport toward the interior. The widening could, however, be an artifact of the eddy parameterization [*Bentsen et al*., 2013; *Eden et al*., 2009; *Eden and Greatbatch*, 2008], which increases horizontal diffusivity when the buoyancy frequency increases as happens with increasing runoff and stronger stratification.

Interestingly, although the AW layer circulation strengthens inside the Arctic Ocean, the net exchange through the gateways generally weakens as seen in section 3.3. From the mass conservation point of view, a stronger boundary current does not require larger AW inflow if there is a reorganization of the circulation. In the 2.0 runoff experiment, we see such a reorganization, with the AW inflow continuing as a boundary current around the Arctic Ocean instead of recirculating within the Eurasian Basin as in the control simulation (Figure 8 and supporting information Figure S3). Qualitatively, the circulation response to increasing river runoff resembles the response to positive AO forcing, with a weaker Beaufort Gyre and a stronger boundary current [*Karcher et al*., 2012].

### 3.3. Volume and Heat Exhanges Between Arctic Ocean and Surrounding Basins

The volume exchange through the Arctic gateways generally weakens as the runoff increases. This is true for the net volume transport in the Bering Strait, CAA, and BSO (Figure 13a). There is an increase in net volume transport in the Fram Strait reaching 0.5 Sv (approximately 40%) in the highest runoff case.

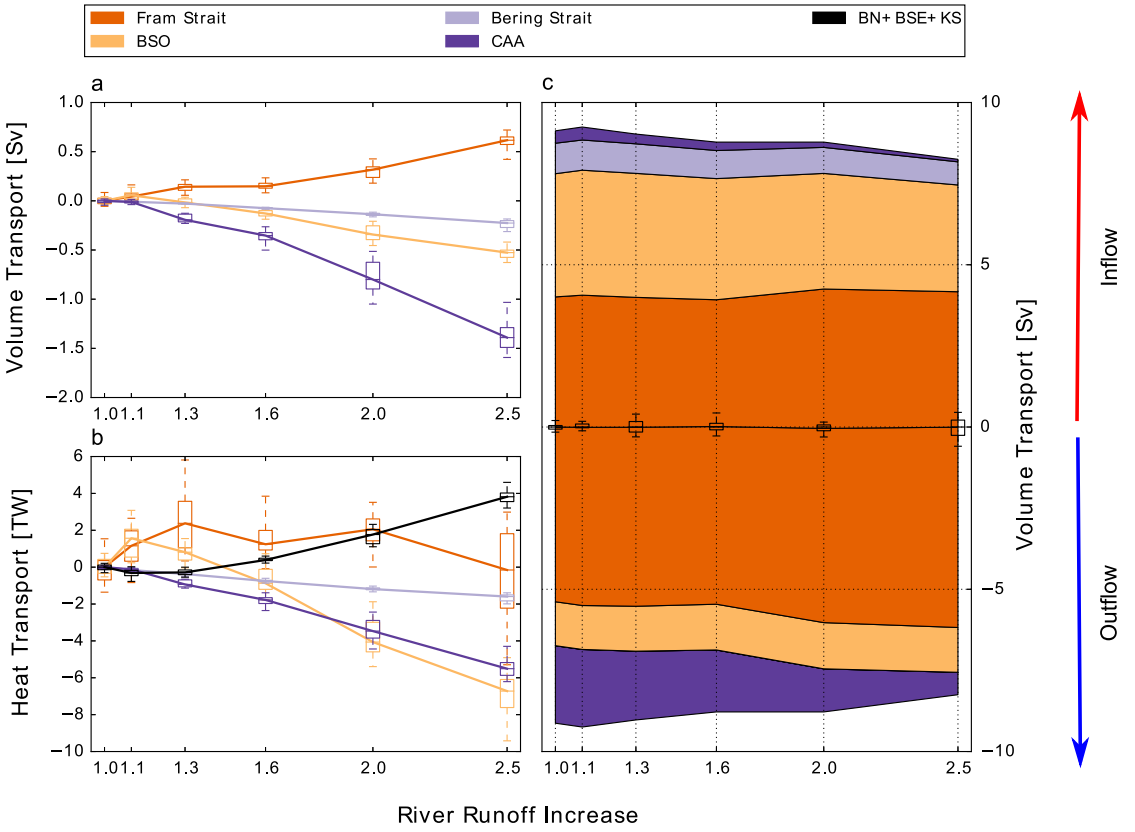


**Figure 13.** Transport through the Arctic gateways as a function of runoff shown as anomalies relative to the control simulation: (a) net volume transport, (b) net heat transport calculated relative to 0°C, and (c) volume transport components (negative values indicate outflow and positive values indicate inflow to the Arctic Ocean). Whisker-and-box symbols show the extreme and interquartile ranges during the 20 year analysis period, and the solid line connects the medians. The mean volume and heat transport values for the control simulation are given in Table 1. The BN+BSE+KS component is the transport through the northern and eastern end of the Barents Sea. The volume transport is not shown for this section as it matches the volume transport in the BSO; the mean net heat transport (±standard deviation) in the control simulation is −16.02±0.16 TW.

The general weakening of the volume exchanges can be understood in terms of how increasing runoff alters SSH and pressure gradients across the gateways [*McGeehan and Maslowski*, 2012]. With more runoff, the surface freshens and SSH increases inside the Arctic Ocean (Figure 14), thus weakening the pressure gradient that drives the inflow through the Bering Strait. In addition, freshwater accumulates in Baffin Bay, thus weakening the pressure gradient that drives outflow through the CAA. At the same time, changes in the sea surface gradients orient the transpolar drift toward Fram Strait rather than CAA (see section 3.2). As a result, the net volume transports weaken through both the Bering Strait and CAA by 25% and 50%, respectively, in the highest runoff case compared to the control simulation (Figure 13a). The decrease in outflow through the CAA is about 1 Sv larger than the decrease in inflow through the Bering Strait, but the net exchange is balanced by the surface outflow through Fram Strait (Figure 13c).

The inflows through the Fram Strait and Barents Sea are closely coupled because they are both branches of the AW inflow, which divides just upstream of the BSO. The sum of the inflows remains close to constant with increasing runoff (Figure 13c) which is to be expected as there is no large change in the AW inflow (North Atlantic Drift) through the Nordic Seas (Figure 12).

The changes in the net heat transports through the gateways generally follow the changes in volume transports. The heat transport decreases in the Bering Strait, CAA, and BSO with the decreasing volume transport (Figure 13b). Heat transport through the Fram Strait stays close to constant despite an increase in volume transport, because the negative heat transport anomaly due to the colder inflow is compensated by a stronger cold outflow, which is a positive heat transport when referenced to 0°C. More locally, the heat transport through the BSO decreases, but in the northern and eastern exits, it increases due to reduced surface cooling (not shown) and reduced volume transport through the Barents Sea. The overall ocean heat transport to the Arctic Ocean decreases from 97 ± 1.0 to 83 ± 4.5 TW over the 1.0–2.5 runoff experiments.

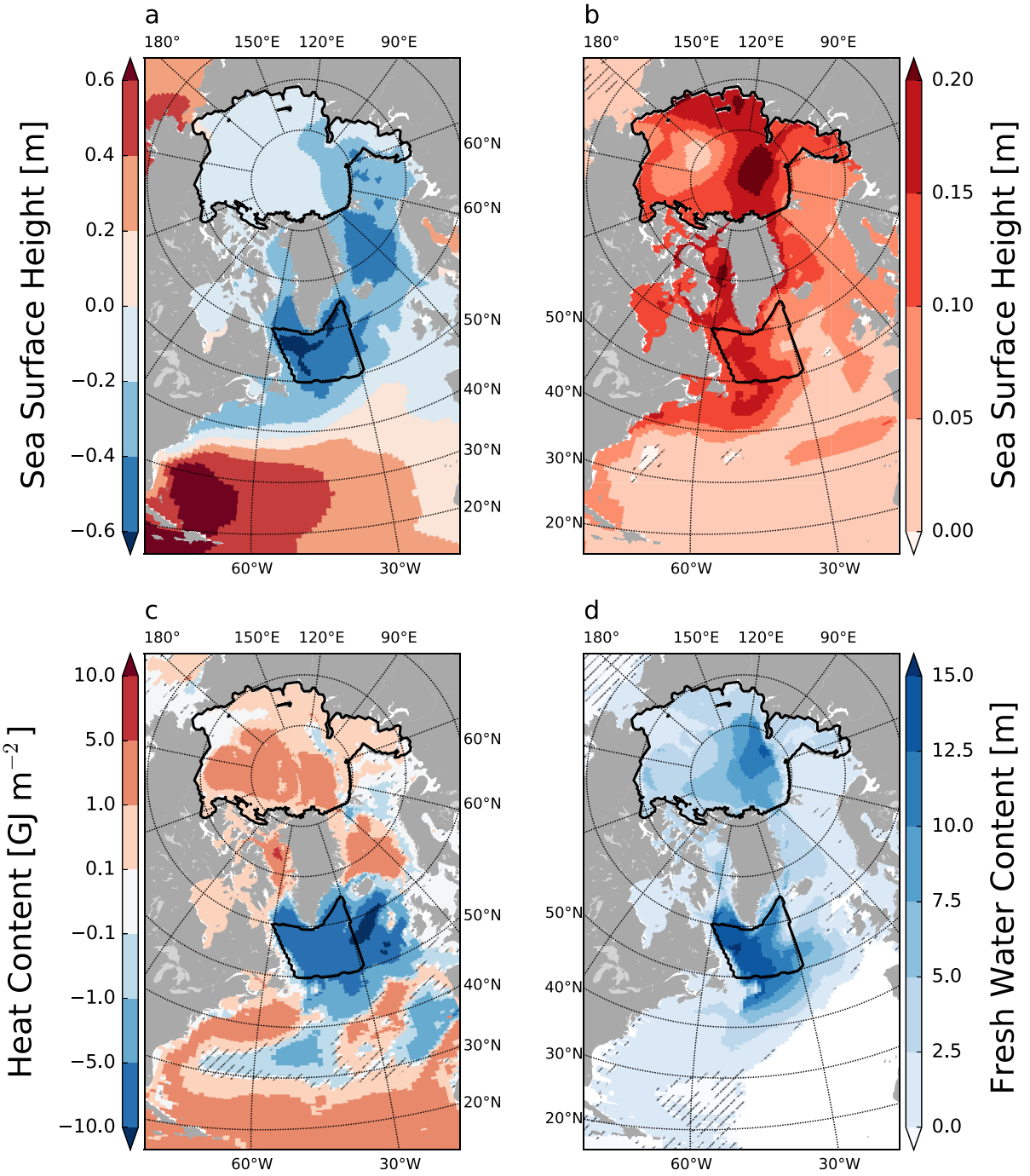


**Figure 14.** (a) Sea surface height in the control simulation and anomalies in the (b) 2.0 runoff experiment of sea surface height, (c) vertically integrated heat content, and (d) vertically integrated freshwater content. Freshwater content is calculated relative to a salinity of 34.8. Hatching indicates values that are not significantly different from the control simulation at the 95% confidence level. The solid black line indicates the regions in the Arctic and subpolar gyre area which were used to calculate the heat budgets in Figure 16.

### 3.4. Regional Response Outside the Arctic Ocean Due to Increased Runoff

At large scales in the North Atlantic, the anomalies in freshwater content (Figure 14d) compare well with the (absolute) anomalies in the barotropic stream function (Figure 12a) because the two are coupled via the SSH: changes in freshwater content alter ocean density and SSH gradients, which in turn affect the barotropic circulation. In the Nordic Seas, the increased outflow from Fram Strait generally freshens the basin, especially around the rims, which enhances local SSH gradients (Figure 14b). This strengthens the

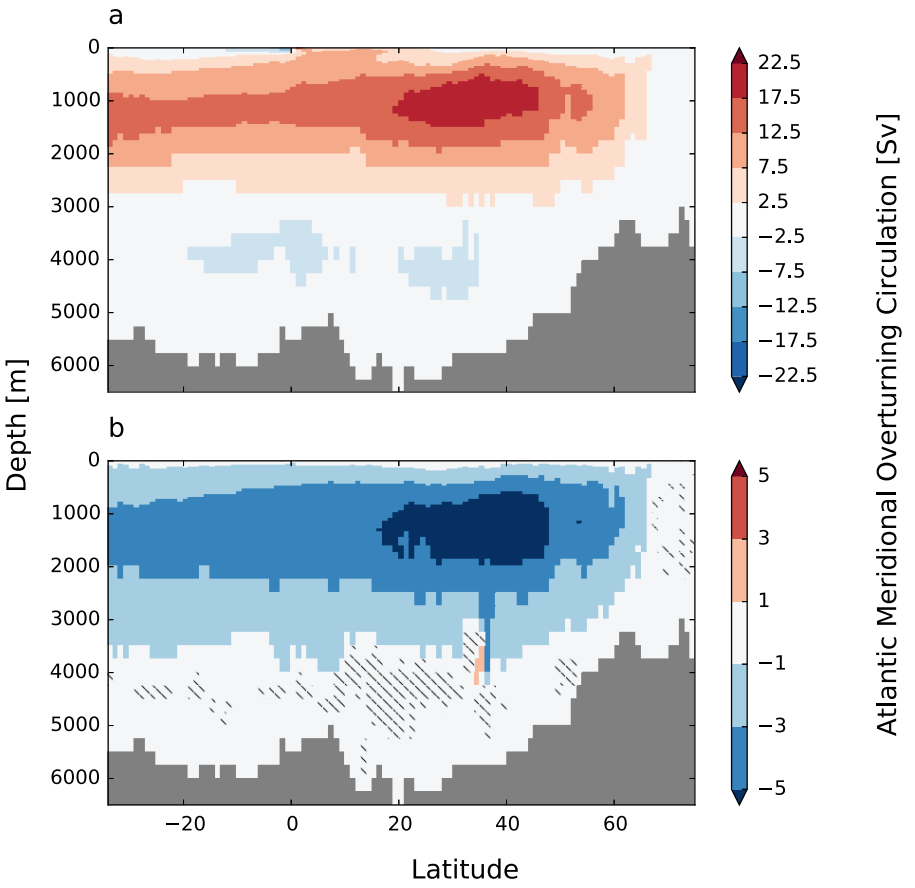


**Figure 15.** (a) Atlantic Meriodional Overturning Circulation (AMOC) in the control simulation and (b) AMOC anomaly in the 2.0 runoff experiment. AMOC is the stream function calculated in the Atlantic Basin in depth coordinates. Hatching indicates values that are not significantly different from the control simulation at the 95% confidence level.

barotropic circulation and intensifies the East Greenland Current in particular (Figure 12). Further south, the subpolar gyre region freshens as more freshwater is brought in from the Arctic Ocean, and less saline Atlantic Water is brought in from the south. A fresher surface layer leads to lighter convective water masses and weakens the gradients of isopycnal surfaces and SSH between the subpolar gyre and subtropical North Atlantic, leading to flatter isopycnals and a weaker barotropic circulation.

As the water masses produced by convection become increasingly fresher and lighter, they weaken the deep western boundary current and the AMOC. In the 2.0 Arctic runoff experiment, there is a 8 Sv (36%) reduction in the AMOC (Figure 15) by the end of the simulation with a continued trend of approximately 1.5 Sv/decade during the 20 year analysis period. Convection continues in the Labrador Sea throughout the simulation.

Finally, we note that while the large-scale warming in the Arctic Ocean is a result of reduced ocean-to-atmosphere heat loss due to stronger stratification, the subpolar latitudes cool due to reduced heat transport convergence. Within the Arctic, ocean heat transport convergence (HCONV) is relatively stable as a function of runoff (Figure 16a), yet the heat content tendency (dH/dt) and heat content anomaly ($\Delta$H) indicate consistent warming with more runoff. This can only be possible with a reduction in surface heat fluxes (HSFC). Because the atmospheric forcing is fixed, the change in surface heat flux must be due to oceanic changes, namely stronger stratification. In the subpolar gyre region, there is a decrease in ocean heat transport convergence (weaker inflow of warm water from the south) that drives a cooling of the ocean and a decrease in surface heat flux that is a response to reduced temperature difference between the atmosphere and the (cooler) ocean (Figure 16b). In terms of the heat budget changes, the western Nordic Seas are similar to the Arctic Ocean, while the eastern Nordic Seas are similar to the subpolar gyre region (not shown). The heat budget in Figure 16 also reveals that the ocean heat content has not equilibrated as the heat content tendency is nonzero during the analysis period.

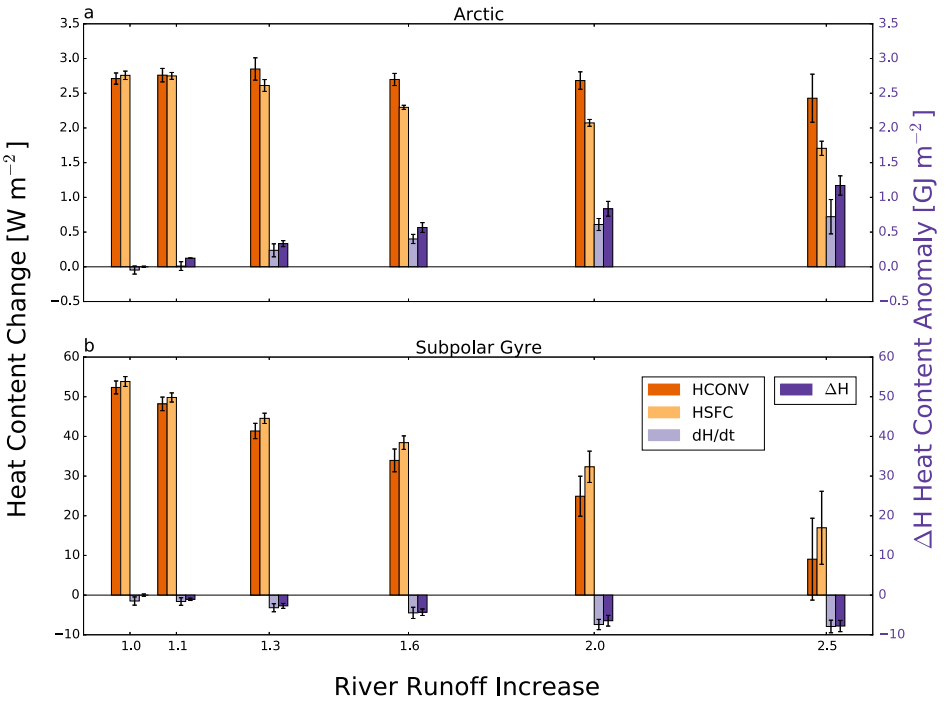


**Figure 16.** Annual mean heat budget in the (a) Arctic and (b) subpolar gyre region. HCONV (W m$^{-2}$) is the depth-integrated ocean heat transport convergence, HSFC (W m$^{-2}$) is the net surface heat flux (positive when ocean is losing heat), dH/dt (W m$^{-2}$) is the local change in heat content, and ΔH (GJ m$^{-2}$) is the heat content anomaly relative to the control simulation. The black bars show the standard deviation. Note the different scales on *y* axis in the two plots. See Figure 14 for the boundaries of the Arctic and subpolar gyre region.

## 4. Discussion

### 4.1. Local Arctic Response

Within the Arctic, the control simulation and the response to increasing runoff appear reasonable when compared to observations in terms of net exchanges through the Arctic gateways (Table 1) and circulation patterns within the Arctic Ocean (Figure 12 and supporting information Figure S3). The simulated response to increasing Arctic runoff is consistent with accepted theoretical ideas: changes in transports are linked to changes in freshwater content and SSH gradients, and can be explained by barotropic arguments (section 3.3). The changes in heat content can be explained by changes in stratification and ocean heat transport (section 3.4, Figure 16).

The cold halocline is not well represented in the control simulation's basin-wide vertical profiles (Figure 6), but results indicate that some of the related processes are acting correctly. The coldest halocline temperatures in the central Arctic are off the Barents Sea and the Siberian shelves (Figures 10c and 10d), consistent with the local winter convection and flow of cold, dense shelf waters toward the interior Arctic Ocean, as postulated by *Rudels et al*. [1996] and *Steele and Boyd* [1998]. The model is likely producing overly dense shelf waters and mixing them too efficiently with the AW layer, but the fact that the shelf waters are formed in the correct regions and subsequently follow realistic pathways toward the interior gives some confidence that the response to freshwater forcing is qualitatively correct.

The recent observations of warmer AW layer temperatures [*Seidov et al*., 2014] have been linked to warmer AW inflow at Fram Strait [*Beszczynska-Möller et al*., 2012] as well as further south in the Nordic Seas [*Seidov et al*., 2014; *Yashayaev and Seidov*, 2015], rather than to stronger stratification as simulated in our experiments. The warmer inflow is connected to the atmospheric and oceanic conditions in the northern North Atlantic, specifically, the state of the North Atlantic Oscillation and Atlantic Multidecadal Oscillation [*Seidov et al*., 2014; *Yashayaev and Seidov*, 2015]. There could be a role for stronger local stratification in warming the AW layer inside the Arctic Ocean in the future, as discussed by *Polyakov et al*. [2011], although there is not yet any observational support for this. Our simulations suggest that an intensifying warm anomaly inside the Arctic Ocean would be an indication of the local stratification suppressing the vertical heat fluxes.

The strengthening of the AW boundary current with stronger stratification is consistent with previous idealized studies. *Lique et al*. [2015] found that a wider boundary current with a larger transport can be produced by reduced surface stress. *Spall* [2013] suggested that the boundary current is mainly driven by the salinity (density) contrast between the AW and surface layer. In our experiments, increasing runoff enhances the vertical salinity gradients (as in *Spall* [2013]), weakens the Beaufort Gyre (equivalent to reduction in the surface stress in *Lique et al*. [2015]), and produces larger transport in a wider baroclinic boundary current. Recent observations also indicate that the boundary current strength is increasingly controlled by the density gradient-driven baroclinic flow when moving from the Fram Strait toward the interior of the Arctic Ocean [*Pnyushkov et al*., 2015].

### 4.2. Regional Response Within the Surrounding Oceans

Contrary to the traditional estuarine circulation theory [*Stigebrandt*, 1981], the total exchange between the Arctic and surrounding basins goes down as the runoff increases (Figure 13c). As described in section 3.3, the increased inflow in the Fram Strait results from a reorganization of the Atlantic inflow in the Barents Sea and Fram Strait branches (the total inflow in the two branches remains close to constant over the range of runoff perturbations tested). Due to recirculation in the Fram Strait, the inflow amount is sensitive to the exact location of the cross section over which it is measured, but the response to increasing runoff is similar independent of the location.

While we see no evidence of an estuarine response in our experiments, it could be masked by changes in the overall circulation pattern. In fact, in the smallest runoff case (1.1 runoff experiment), when the circulation changes are also smallest, the model simulates a slight increase in total exchange (Figure 13c), consistent with estuarine circulation theory.

The decrease in the Barents Sea throughflow is explained by freshwater accumulation in the Eurasian Basin (Figure 14). This freshwater accumulation increases the SSH in the Eurasian Basin, which decreases the barotropic pressure gradient over the Barents Sea. This is consistent with the postulated ocean feedback [*Smedsrud et al*., 2013] where rising sea level to the north would decrease AW inflow in the BSO.

The changes in the inflows and outflows have some important consequences for the freshwater accumulation in the subpolar gyre. Earlier observational and high-resolution model studies have shown that mixing from the West Greenland Current (source from Fram Strait via the East Greenland Current) toward the central Labrador sea is much larger than from the Labrador Current (source from CAA) [*Myers*, 2005; *Schmidt and Send*, 2007; *Kawasaki and Hasumi*, 2014]. This implies that a freshwater perturbation flowing out from the Arctic mainly via the Fram Strait (as in our simulations) has a larger impact on the Labrador Sea convection sites, subpolar gyre circulation, and the AMOC, than a freshwater perturbation flowing out via the CAA [see also *Condron and Winsor*, 2012, Figure 2].

The AMOC weakens with increasing runoff despite ongoing convection both in the Labrador and Greenland Seas. Reduction in the AMOC is a well-documented result in North Atlantic hosing experiments [*Manabe and Stouffer*, 1995; *Stouffer et al*., 2006; *Stocker et al*., 2007; *Mignot et al*., 2007; *Roche et al*., 2010] as well as Arctic freshwater perturbations [*Peltier et al*., 2006; *Rennermalm et al*., 2006, 2007]. However, in many of these hosing experiments, the AMOC reduction is associated with a complete shutdown of convection in the North Atlantic, which is not the case in our simulations.

### 4.3. Limitations of the Study

Our model setup has clear biases in the Arctic. There are large discrepancies in the simulated salinities and AW layer temperature compared with observations (Figures 5 and 6), although we do not expect an exact match because of our idealized atmospheric forcing. However, the simulated large-scale response to increased runoff is consistent over a range of runoff perturbations, providing some confidence in the results despite the biases in the mean state. The mechanisms we identify are similar to those in a number of previous studies using other model systems [*Lique et al*., 2015; *Spall*, 2013], though the details are likely to be model dependent.

A clear limitation of our study is the model resolution (1° horizontal resolution), which is too coarse to properly represent narrow currents and requires subgrid-scale phenomena (such as eddies) to be parameterized. This adds uncertainties to our estimate of runoff sensitivity. For example, the model simulates a broad Arctic boundary current rather than a narrow, bottom-trapped feature, meaning that the gradients are quite

different, and hence their response to increasing runoff could also be quite different. The model also simulates a broader East Greenland Current (EGC) than is observed. This could result in too much freshwater mixing to the interior Nordic Seas and Labrador Sea from the EGC, with implications for convection and water mass transformation. The large grid size also affects the freshwater pathways inside the Arctic, changing the simulated regional response. For example, the model does not resolve coastal currents, which can be important for the freshwater transports [*Janout et al*., 2015; *Whitefield et al*., 2015]. However, we think that while these features are important at regional scales, the simulated basin-wide response is qualitatively robust at multidecadal time scales.

Another consideration is that our atmospheric forcing does not include interannual variability. We chose to force the model with an idealized climatological atmosphere because our aim was to understand the time-averaged ocean and sea ice response to increasing Arctic river runoff. This climatology is close to neutral in terms of the Arctic Oscillation (AO), the primary pattern of variability in the extratropical Northern Hemisphere. Because the AO affects surface circulation, one might expect different AO conditions to result in different pathways for river runoff and hence, different responses to runoff perturbations. We ran an additional sensitivity experiment with doubled runoff for an extremely positive AO year (1989; not shown) and find similar results as in the 2.0 runoff experiment, suggesting that the response is not qualitatively dependent on the atmospheric state. Finally, we have left out any comparison between the strength of the AO-driven interannual variability and the runoff-driven changes, mainly because there is large uncertainty in terms of future changes in AO variability.

## 5. Conclusions

We have shown that realistic Arctic freshwater perturbations can cause notable changes both inside and outside the Arctic Ocean. The main Arctic response to increased river runoff is a fresher surface and stronger stratification with a warmer halocline and a warmer Atlantic Water layer. In accordance with earlier idealized studies, we find a strengthening of the cyclonic circulation inside the Arctic Ocean Atlantic Water layer. Freshwater accumulates in the Eurasian Basin and raises sea level locally, leading to reduced inflow to the Arctic Ocean through the Bering Strait and the Barents Sea. Freshwater also accumulates and raises sea level in Baffin Bay, leading to reduced outflow through the Canadian Arctic Archipelago. Overall there is a small decrease in the total exchange between the Arctic Ocean and the surrounding seas with increased runoff, contrary to expectations from estuarine circulation theory.

Outside the Arctic Ocean, the additional freshwater affects water mass transformation in the subpolar gyre region. For a doubling of runoff, the gyre circulation slows down by more than 10 Sv (25%) at its maximum, and the Atlantic Meridional Overturning Circulation slows down by about 8 Sv (36%) by the end of the simulations, with a downward trend of approximately 1.5 Sv/decade. Despite considerable freshwater accumulation in the subpolar gyre, there is ongoing convection in the region.

While our results are robust over a range of runoff perturbations in a coupled sea ice-ocean model, the missing atmospheric feedbacks should be assessed in future studies. In particular, a changing sea ice cover affects pressure and wind patterns through thermodynamic and mechanical coupling, and this in turn could influence the sea ice and ocean circulation. Similarly, the changing albedo could affect the global energy balance and hence atmospheric and oceanic circulation on larger scales. Although the atmospheric feedbacks would likely modulate the strength and timing of the simulated responses, a strong freshwater perturbation could still be expected to force an ocean response similar to that documented in this study.

There is a strong model-based evidence that high-latitude freshwater perturbations affect ocean circulation in the North Atlantic and Arctic, though the details of the response can be model dependent. There is also ample observational and paleo proxy evidence suggesting similar linkages. Our results suggest that the response to high-latitude freshwater perturbations can be very different close to the source regions compared with further south at subpolar latitudes. Future work should aim to understand the differences in the regional response to freshwater perturbations in coupled models and in proxy records. It would be highly valuable, although challenging, to reconstruct magnitudes of the past freshwater forcing events and combine those estimates with high-resolution coupled models.

**Acknowledgments**

We wish to thank M. Bentsen and I. Bethke for help with the model setup and B. Tremblay, L. Renaud-Desjardins, and E. Lambert for insightful discussions and helpful comments. We would also like to thank C. Lique, one anonymous reviewer, and the Editor for useful comments that helped improve the manuscript. We acknowledge the World Climate Research Programme's Working Group on Coupled Modelling, which is responsible for CMIP, for data, and we thank the climate modeling groups (listed in supporting information Table S1 of this paper) for producing and making available their model output. For CMIP, the U.S. Department of Energy's Program for Climate Model Diagnosis and Intercomparison provides coordinating support and led development of software infrastructure in partnership with the Global Organization for Earth System Science Portals. All the data, model setup, and analysis scripts used in this study are available through the corresponding author by e-mail at aleksi.nummelin@uib.no. M. Ilicak is supported by Ice2Ice project that has received funding from the European Research Council under the European Community's Seventh Framework Programme (FP7/2007-2013)/ERC grant agreement 610055. This work was supported by the Bjerknes Centre projects DYNAWARM and BASIC and the Centre for Climate Dynamics (SKD) at the Bjerknes Centre (C. Li).

## References

Alkire, M. B., J. Morison, and R. Andersen (2015), Variability in the meteoric water, sea-ice melt, and Pacific water contributions to the central Arctic Ocean, 2000–2014, *J. Geophys. Res. Oceans*, *120*, 1573–1598, doi:10.1002/2014JC010023.

Bauch, D., J. A. Hölemann, A. Nikulina, C. Wegner, M. A. Janout, L. A. Timokhov, and H. Kassens (2013), Correlation of river water and local sea-ice melting on the Laptev Sea shelf (Siberian Arctic), *J. Geophys. Res. Oceans*, *118*, 550–561, doi:10.1002/jgrc.20076.

Bentsen, M., et al. (2013), The Norwegian Earth System Model, NorESM1-M—Part 1: Description and basic evaluation of the physical climate, *Geosci. Model Dev.*, *6*(3), 687–720, doi:10.5194/gmd-6-687-2013.

Beszczynska-Möller, A., E. Fahrbach, U. Schauer, and E. Hansen (2012), Variability in Atlantic water temperature and transport at the entrance to the Arctic Ocean, 1997–2010, *ICES J. Mar. Sci.*, *69*(5), 852–863, doi:10.1093/icesjms/fss056.

Bleck, R., and L. T. Smith (1990), A wind-driven isopycnic coordinate model of the north and equatorial Atlantic Ocean: 1. Model development and supporting experiments, *J. Geophys. Res.*, *95*(C3), 3273–3285, doi:10.1029/JC095iC03p03273.

Bleck, R., C. Rooth, D. Hu, and L. T. Smith (1992), Salinity-driven thermocline transients in a wind- and thermohaline-forced isopycnic coordinate model of the north Atlantic, *J. Phys. Oceanogr.*, *22*(12), 1486–1505, doi:10.1175/1520-0485(1992)022⟨1486:SDTTIA⟩2.0.CO;2.

Condron, A., and P. Winsor (2012), Meltwater routing and the Younger Dryas, *Proc. Natl. Acad. Sci. U.S.A.*, *109*(49), 19,928–19,933, doi:10.1073/pnas.1207381109.

Deshayes, J., R. Curry, and R. Msadek (2014), CMIP5 model intercomparison of freshwater budget and circulation in the North Atlantic, *J. Clim.*, *27*, 3298–3317, doi:10.1175/JCLI-D-12-00700.1.

Dmitrenko, I. A., et al. (2010), Wind-driven diversion of summer river runoff preconditions the Laptev Sea coastal polynya hydrography: Evidence from summer-to-winter hydrographic records of 2007–2009, *Cont. Shelf Res.*, *30*(15), 1656–1664, doi:10.1016/j.csr.2010.06.012.

Droettboom, M., et al. (2015), matplotlib: v1.4.3, doi:10.5281/zenodo.15423.

Eden, C., and R. J. Greatbatch (2008), Towards a mesoscale eddy closure, *Ocean Modell.*, *20*(3), 223–239, doi:10.1016/j.ocemod.2007.09.002.

Eden, C., M. Jochum, and G. Danabasoglu (2009), Effects of different closures for thickness diffusivity, *Ocean Modell.*, *26*(1-2), 47–59, doi:10.1016/j.ocemod.2008.08.004.

Fichot, C. G., K. Kaiser, S. B. Hooker, R. M. W. Amon, M. Babin, S. Bélanger, S. A. Walker, and R. Benner (2013), Pan-Arctic distributions of continental runoff in the Arctic Ocean., *Sci. Rep.*, *3*, 1053, doi:10.1038/srep01053.

Gent, P. R., et al. (2011), The community climate system model version 4, *J. Clim.*, *24*(19), 4973–4991, doi:10.1175/2011JCLI4083.1.

Gerdes, R., W. Hurlin, and S. M. Griffies (2006), Sensitivity of a global ocean model to increased run-off from Greenland, *Ocean Modell.*, *12*(3-4), 416–435, doi:10.1016/j.ocemod.2005.08.003.

Holland, M. M., D. A. Bailey, B. P. Briegleb, B. Light, and E. Hunke (2012), Improved sea ice shortwave radiation physics in CCSM4: The impact of melt ponds and aerosols on Arctic sea ice, *J. Clim.*, *25*(5), 1413–1430, doi:10.1175/JCLI-D-11-00078.1.

Hunter, J. D. (2007), Matplotlib: A 2d graphics environment, *Comput. Sci. Eng.*, *9*(3), 90–95, doi:10.1109/MCSE.2007.55.

Janout, M. A., et al. (2015), Kara Sea freshwater transport through Vilkitsky Strait: Variability, forcing, and further pathways toward the western Arctic Ocean fromamodel and observations Markus, *J. Geophys. Res. Oceans*, *120*, 2331–2349, doi:10.1002/2014JC010632.

Jones, E. P. (2001), Circulation in the Arctic Ocean, *Polar Res.*, *20*(2), 139–146, doi:10.1111/j.1751-8369.2001.tb00049.x.

Karcher, M., F. Kauker, R. Gerdes, E. Hunke, and J. Zhang (2007), On the dynamics of Atlantic Water circulation in the Arctic Ocean, *J. Geophys. Res.*, *112*, C04S02, doi:10.1029/2006JC003630.

Karcher, M., J. N. Smith, F. Kauker, R. Gerdes, and W. M. Smethie (2012), Recent changes in Arctic Ocean circulation revealed by iodine-129 observations and modeling, *J. Geophys. Res.*, *11*, C08007, doi:10.1029/2011JC007513.

Kawasaki, T., and H. Hasumi (2014), Effect of freshwater from the West Greenland Current on the winter deep convection in the Labrador Sea, *Ocean Modell.*, *75*, 51–64, doi:10.1016/j.ocemod.2014.01.003.

Komuro, Y. (2014), The impact of surface mixing on the Arctic river water distribution and stratification in a global ice-ocean model, *J. Clim.*, *27*, 4359–4370, doi:10.1175/JCLI-D-13-00090.1.

Large, W. G., and S. G. Yeager (2004), Diurnal to decadal global forcing for ocean and sea–ice models: The data sets and flux climatologies, NCAR/TN-460+STR Technical note, NCAR, doi:10.5065/D6KK98Q6.

Lehner, F., C. C. Raible, D. Hofer, and T. F. Stocker (2012), The freshwater balance of polar regions in transient simulations from 1500 to 2100 AD using a comprehensive coupled climate model, *Clim. Dyn.*, *39*(1-2), 347–363, doi:10.1007/s00382-011-1199-6.

Lique, C., H. L. Johnson, and P. E. Davis (2015), On the interplay between the circulation in the surface and the intermediate layers of the Arctic Ocean, *J. Phys. Oceanogr.*, *45*, 1393–1409, doi:10.1175/JPO-D-14-0183.1.

Locarnini, R. A., et al. (2013), *World Ocean Atlas 2013, vol. 1, Temperature, NOAA Atlas NESDIS 73*, edited by S. Levitus and A. Mishonov, 40 pp. [Available at http://data.nodc.noaa.gov/woa/WOA13/DOC/woa13_vol1.pdf.]

Manabe, S., and R. Stouffer (1995), Simulation of abrupt climate change induced by freshwater input to the North Atlantic Ocean, *Nature*, *378*, 165–167, doi:10.1038/378165a0.

McGeehan, T., and W. Maslowski (2012), Evaluation and control mechanisms of volume and freshwater export through the Canadian Arctic Archipelago in a high-resolution pan-Arctic ice-ocean model, *J. Geophys. Res.*, *117*, C00D14, doi:10.1029/2011JC007261.

Melling, H., et al. (2008), Fresh-water fluxes via Pacific and Arctic outflows across the Canadian Polar Shelf, in *Arctic–Subarctic Ocean Fluxes*, edited by R. R. Dickson, J. Meincke, and P. Rhines, pp. 193–247, Springer, Dordrecht, Netherlands, doi:10.1007/978-1-4020-6774-7_10.

Mignot, J., A. Ganopolski, and A. Levermann (2007), Atlantic subsurface temperatures: Response to a shutdown of the overturning circulation and consequences for its recovery, *J. Clim.*, *20*(19), 4884–4898, doi:10.1175/JCLI4280.1.

Morison, J., R. Kwok, C. Peralta-Ferriz, M. Alkire, I. Rigor, R. Andersen, and M. Steele (2012), Changing Arctic Ocean freshwater pathways, *Nature*, *481*(7379), 66–70, doi:10.1038/nature10705.

Myers, P. G. (2005), Impact of freshwater from the Canadian Arctic Archipelago on Labrador Sea Water formation, *Geophys. Res. Lett.*, *32*, 1–4, doi:10.1029/2004GL022082.

Nghiem, S. V., D. K. Hall, I. Rigor, P. Li, and G. Neumann (2014), Effects of Mackenzie River discharge and bathymetry on sea ice in the Beaufort Sea, *Geophys. Res. Lett.*, *41//*, 873–879, doi:10.1002/2013GL058956.

Nguyen, A. T., D. Menemenlis, and R. Kwok (2009), Improved modeling of the Arctic halocline with a subgrid-scale brine rejection parameterization, *J. Geophys. Res.*, *114*, C11014, doi:10.1029/2008JC005121.

Nilsson, J., and G. Walin (2010), Salinity-dominated thermohaline circulation in sill basins: Can two stable equilibria exist?, *Tellus, Ser. A*, *62*(2), 123–133, doi:10.1111/j.1600-0870.2009.00428.x.

Nummelin, A., C. Li, and L. H. Smedsrud (2015), Response of Arctic Ocean stratification to changing river runoff in a column model, *J. Geophys. Res. Oceans*, *120*, 2655–2675, doi:10.1002/2014JC010571.

Overeem, I., and J. P. M. Syvitski (2010), Shifting discharge peaks in Arctic Rivers, 1977–2007, *Geogr. Ann., Ser. A*, *92*(2), 285–296, doi:10.1111/j.1468-0459.2010.00395.x.
Peltier, W. R., G. Vettoretti, and M. Stastna (2006), Atlantic meridional overturning and climate response to Arctic Ocean freshening, *Geophys. Res. Lett.*, *33*, L06713, doi:10.1029/2005GL025251.
Pemberton, P., J. Nilsson, M. Hieronymus, and H. M. Meier (2015), Arctic Ocean water mass transformation in S–T coordinates, *J. Phys. Oceanogr.*, *45*(4), 1025–1050, doi:10.1175/JPO-D-14-0197.1.
Peterson, B. J., R. M. Holmes, J. W. McClelland, C. J. Vörösmarty, R. B. Lammers, A. I. Shiklomanov, I. A. Shiklomanov, and S. Rahmstorf (2002), Increasing river discharge to the Arctic Ocean., *Science*, *298*(5601), 2171–2173, doi:10.1126/science.1077445.
Pnyushkov, A. V., I. V. Polyakov, V. V. Ivanov, Y. Aksenov, A. C. Coward, M. Janout, and B. Rabe (2015), Structure and variability of the boundary current in the Eurasian Basin of the Arctic Ocean, *Deep Sea Res., Part I*, *101*, 80–97, doi:10.1016/j.dsr.2015.03.001.
Polyakov, I. V., et al. (2011), Fate of early 2000s Arctic warm water pulse, *Bull. Am. Meteorol. Soc.*, *92*(5), 561–566, doi:10.1175/2010BAMS2921.1.
Rawlins, M. A., et al. (2010), Analysis of the Arctic system for freshwater cycle intensification: Observations and expectations, *J. Clim.*, *23*(21), 5715–5737, doi:10.1175/2010JCLI3421.1.
Rennermalm, A. K., E. F. Wood, S. J. Déry, A. J. Weaver, and M. Eby (2006), Sensitivity of the thermohaline circulation to Arctic Ocean runoff, *Geophys. Res. Lett.*, *33*, L12703, doi:10.1029/2006GL026124.
Rennermalm, A. K., E. F. Wood, A. J. Weaver, M. Eby, and S. J. Déry (2007), Relative sensitivity of the Atlantic meridional overturning circulation to river discharge into Hudson Bay and the Arctic Ocean, *J. Geophys. Res.*, *112*, G04S48, doi:10.1029/2006JG000330.
Rennermalm, A. K., E. F. Wood, and T. J. Troy (2010), Observed changes in pan-Arctic cold-season minimum monthly river discharge, *Clim. Dyn.*, *35*(6), 923–939, doi:10.1007/s00382-009-0730-5.
Roche, D. M., A. P. Wiersma, and H. Renssen (2010), A systematic study of the impact of freshwater pulses with respect to different geographical locations, *Clim. Dyn.*, *34*, 997–1013, doi:10.1007/s00382-009-0578-8.
Rudels, B. (2015), Arctic Ocean circulation, processes and water masses: A description of observations and ideas with focus on the period prior to the International Polar Year 2007–2009, *Prog. Oceanogr.*, *132*, 22–67, doi:10.1016/j.pocean.2013.11.006.
Rudels, B., L. G. Anderson, and E. P. Jones (1996), Formation and evolution of the surface mixed layer and halocline of the Arctic Ocean, *J. Geophys. Res.*, *101*(C4), 8807–8821, doi:10.1029/96JC00143.
Rudels, B., E. P. Jones, U. Schauer, and P. B. Eriksson (2004), Atlantic sources of the Arctic Ocean surface and halocline waters, *Polar Res.*, *23*(2), 181–208, doi:10.1111/j.1751-8369.2004.tb00007.x.
Schauer, U., A. Beszczynska-Möller, W. Walczowski, E. Fahrbach, J. Piechura, and E. Hansen (2008), Variation of measured heat flow through the Fram Strait between 1997 and 2006, in *Arctic–Subarctic Ocean Fluxes*, edited by R. R. Dickson, J. Meincke, and P. Rhines, pp. 65–85, Springer, Dordrecht, Netherlands, doi:10.1007/978-1-4020-6774-7_4.
Schlosser, P., D. Bauch, R. Fairbanks, and G. Bönisch (1994), Arctic river-runoff: Mean residence time on the shelves and in the halocline, *Deep Sea Res., Part I*, *41*(7), 1053–1068, doi:10.1016/0967-0637(94)90018-3.
Schmidt, S., and U. Send (2007), Origin and composition of seasonal Labrador Sea freshwater, *J. Phys. Oceanogr.*, *37*(6), 1445–1454, doi:10.1175/JPO3065.1.
Schmidtko, S., G. C. Johnson, and J. M. Lyman (2013), MIMOC: A global monthly isopycnal upper-ocean climatology with mixed layers, *J. Geophys. Res. Oceans*, *118*, 1658–1672, doi:10.1002/jgrc.20122.
Seidov, D., J. I. Antonov, K. M. Arzayus, O. K. Baranova, M. Biddle, T. P. Boyer, D. R. Johnson, A. V. Mishonov, C. Paver, and M. M. Zweng (2014), Oceanography north of 60˚N from World Ocean Database, *Prog. Oceanogr.*, *132*, 153–173, doi:10.1016/j.pocean.2014.02.003.
Smedsrud, L. H., et al. (2013), The role of the Barents Sea in the Arctic climate system, *Rev. Geophys.*, *51*(3), 415–449, doi:10.1002/rog.20017.
Spall, M. A. (2013), On the circulation of Atlantic Water in the Arctic Ocean, *J. Phys. Oceanogr.*, *43*(11), 2352–2371, doi:10.1175/JPO-D-13-079.1.
Steele, M., and T. J. Boyd (1998), Retreat of the cold halocline layer in the Arctic Ocean, *J. Geophys. Res.*, *103*(C5), 10,419–10,435, doi:10.1029/98JC00580.
Steele, M., R. Morley, and W. Ermold (2001), PHC: A global ocean hydrography with a high-quality Arctic Ocean, *J. Clim.*, *14*(9), 2079–2087, doi:10.1175/1520-0442(2001)014⟨2079:PAGOHW⟩2.0.CO;2.
Stigebrandt, A. (1981), A model for the thickness and salinity of the upper layer in the Arctic Ocean and the relationship between the ice thickness and some external parameters, *J. Phys. Oceanogr.*, *11*(10), 1407–1422, doi:10.1175/1520-0485(1981)011⟨1407:AMFTTA⟩2.0.CO;2.
Stocker, T. F., A. Timmermann, M. Renold, and O. Timm (2007), Effects of salt compensation on the climate model response in simulations of large changes of the Atlantic meridional overturning circulation, *J. Clim.*, *20*(24), 5912–5928, doi:10.1175/2007JCLI1662.1.
Stouffer, R., J. Yin, and J. Gregory (2006), Investigating the causes of the response of the thermohaline circulation to past and future climate changes, *J. Clim.*, *19*(8), 1365–1387, doi:10.1175/JCLI3689.1.
Swingedouw, D., C. B. Rodehacke, S. M. Olsen, M. Menray, Y. Gao, U. Mikolajewicz, and J. Mignot (2014), On the reduced sensitivity of the Atlantic overturning to Greenland ice sheet melting in projections: A multi-model assessment, *Clim. Dyn.*, *44*, 3261–3279, doi:10.1007/s00382-014-2270-x.
Whitefield, J., P. Winsor, J. Mcclelland, and D. Menemenlis (2015), A new river discharge and river temperature climatology data set for the pan-Arctic region, *Ocean Modell.*, *88*, 1–15, doi:10.1016/j.ocemod.2014.12.012.
Woodgate, R. A., K. Aagaard, and T. J. Weingartner (2005), Monthly temperature, salinity, and transport variability of the Bering Strait through flow, *Geophys. Res. Lett.*, *32*, L04601, doi:10.1029/2004GL021880.
Yamamoto-Kawai, M., F. A. McLaughlin, E. C. Carmack, S. Nishino, K. Shimada, and N. Kurita (2009), Surface freshening of the Canada Basin, 2003–2007: River runoff versus sea ice meltwater, *J. Geophys. Res.*, *114*, C00A05, doi:10.1029/2008JC005000.
Yashayaev, I., and D. Seidov (2015), The role of the Atlantic Water in multidecadal ocean variability in the Nordic and Barents Seas, *Prog. Oceanogr.*, *132*, 68–127, doi:10.1016/j.pocean.2014.11.009.
Zweng, M. M., et al. (2013), *World Ocean Atlas 2013, vol. 2, Salinity, NOAA Atlas NESDIS 74*, edited by S. Levitus and A. Mishonov, 39 pp. [Available at http://data.nodc.noaa.gov/woa/WOA13/DOC/woa13_vol2.pdf.]